Thermodynamic Properties of CO_2 Mixtures and Their Applications in Advanced Power Cycles with CO_2 Capture Processes

Hailong Li

Energy Processes
Department of Chemical Engineering and Technology
Royal Institute of Technology
Stockholm, Sweden

KTH, Royal Institute of Technology
School of Chemical Science and Engineering
Department of Chemical Engineering and Technology
Division of Energy Processes
SE-100 44 Stockholm
Sweden

TRITA-CHE Report 2008:58
ISSN 1654-1081
ISBN 978-91-7415-091-9

Hope it is something…

Abstract:

The thermodynamic properties of CO_2 mixtures are essential for the design and operation of CO_2 capture and storage (CCS) systems. A better understanding of the thermodynamic properties of CO_2 mixtures could provide a scientific basis to define a proper guideline of CO_2 purity and impure components for the CCS processes according to technical, safety, and environmental requirements. However, the available accurate experimental data cannot cover the entire operation conditions of the CCS processes. In order to overcome the shortage of experimental data, theoretical modelling and estimation are used as a supplemental approach.

In this thesis, the available experimental data on the thermodynamic properties of CO_2 mixtures were first collected; their applicability and gaps for theoretical model verification and calibration were also determined according to the required thermodynamic properties and operation conditions of CCS. Then, in order to provide recommendations concerning calculation methods for the engineering design of CCS, a total of eight equations of state (EOS) were evaluated for the calculations concerning vapour liquid equilibrium (VLE) and volume of CO_2 mixtures, including N_2, O_2, SO_2, Ar, H_2S, and CH_4.

With the identified equations of state, the preliminary assessment of the impact of impurity was further conducted regarding the thermodynamic properties of CO_2 mixtures and the different processes involved in the CCS system. Results show that the increment of the mole fraction of non-condensable gases would make purification, compression, and condensation more difficult. Comparatively, N_2 can be separated more easily from the CO_2 mixtures than O_2 and Ar. Moreover, a lower CO_2 recovery rate is expected for the physical separation of CO_2/N_2 under the same separation conditions. In addition, the evaluations of the acceptable concentration of non-condensable impurities show that the transport conditions in vessels are more sensitive to the non-condensable impurities, thus, requiring very low concentration of non-condensable impurities in order to avoid two-phase problems.

Meanwhile, the performances of evaporative gas turbine integrated with different CO_2 capture technologies were investigated from both technical and economical aspects. It is concluded that the evaporative gas turbine (EvGT) cycle with chemical absorption capture has a smaller penalty on electrical efficiency, but a lower CO_2 capture ratio than the EvGT cycle with O_2/CO_2 recycle combustion capture. Therefore, although EvGT + chemical absorption has a higher annual cost, it has a lower cost of electricity because of its higher efficiency. However, considering its lower CO_2 capture ratio, EvGT + chemical absorption has a higher cost to capture 1 ton CO_2. In addition, the efficiency of EvGT + chemical absorption can be increased by optimizing Water/Air ratio, increasing the operating pressure of stripper, and adding a flue gas condenser condensing out the excessive water.

Language: English.

Keywords: thermodynamic property, vapour liquid equilibrium, volume, equation of state, interaction parameter, CO_2 mixtures, evaporative gas turbine, chemical absorption, oxy-fuel combustion, cost evaluation, CO_2 capture and storage

Table of Contents

List of Tables

List of Figures

List of Papers and Technical Reports

This thesis is based on the following papers, referred to by the Roman numerals I- VIII, and technical reports, referred to by the Roman numerals IX and X.

Papers (appended):

I. H. Li, X. Ji, J. Yan. A new modification on RK EOS for gaseous CO_2 and gaseous mixtures of CO_2 and H_2O. *International Journal of Energy Research*, 2006. 30:135-148.

II. H. Li, J. Yan. IMPACTS OF IMPURITIES IN CO_2-FLUIDS ON CO_2 TRANSPORT PROCESS. In: *Proceedings of the ASME Turbo Expo 2006*, Barcelona, Spain May 8-11th 2006. Paper No. GT2006-90954.

III. H. Li, J. Yan. PRELIMINARY STUDY ON CO_2 PROCESSING IN CO_2 CAPTURE FROM OXY-FEUL COMBUSTION. In: *Proceedings of the ASME Turbo Expo 2007*, Montreal, Canada May 14-17th 2007. Paper No. GT2007-27845.

IV. H. Li, J. Yan, J. Yan, M. Anheden. Impurity impacts on the purification process in oxy-fuel combustion based CO_2 capture and storage system. *Applied Energy*, 2008, In Press.

V. H. Li, J. Yan, Evaluating cubic equations of state for calculation of vapour-liquid equilibrium of CO_2 and CO_2 mixtures for CO_2 capture and storage processes. *Applied Energy*, 2008, In Press.

VI. H. Li, J. Yan, PERFORMANCE COMPARISON ON THE EVAPORATIVE GAS TURBINE CYCLES COMBINED WITH DIFFERENT CO_2 CAPTURE OPTIONS. Accepted by the *International Green Energy Conference IV*, Beijing, China 2008.

VII. H. Li, S. Flores, J. Yan. Integrating Evaporative Gas Turbine with Chemical Absorption for Carbon Dioxide Capture. Accepted by the *International Green Energy Conference IV*, Beijing, China 2008.

VIII. H. Li, J. Yan, Impacts of Equations of State (EOS) and Impurities on the Volume Calculation of CO_2 Mixtures in the Applications of CO_2 Capture and Storage (CCS) Processes. Manuscript.

Technical Reports (not appended):

I. H. Li, J. Yan, J. Yan, M. Anheden. Evaluation of Existing Methods for the Thermodynamic Property Calculation of CO_2 mixture. KTH-Vattenfall, 2007.

II. H. Li, J. Yan, J. Yan, M. Anheden. Preliminary Assessment of Impurity Impacts of CO_2 mixture on CO_2 Processing and Transport Process. KTH-Vattenfall, 2007.

Acronyms

Nomenclature:

a, b	Parameters in cubic equations of state
a_1, a_2	Parameters of modified RK equation
C, c	Heat capacity *J/(mol·K)*
c_1, …, c_5	Constant to calculate heat capacity
G	Gas
h	Enthalpy *kJ/mol*
k_{ij}	Binary interaction parameter
L	Liquid
M	General representative of parameters
n	Mole number
P	Pressure *MPa*
R	Gas constant *J/(mol·K)*
T	Temperature *K*
V, v	Molar volume *mol/l*
u, w	Parameters in 3P1T equation of state
x	Mole fraction in liquid phase
X	Total mole fraction
y	Mole fraction in vapour phase
Z	Compressibility
α	Relative volatility
ζ	Binary interaction parameter of PT equation of state

Abbreviation:

AAD	Absolute average deviations %
ACCR	Actual CO_2 capture ratio
ASU	Air separation unit
Abs	Absolute value
BP	Bubble point
BWR	Benedict-Webb-Rubin
CC	Combined cycle
CCR	CO_2 capture ratio
CCS	CO_2 capture and storage
Comp	Compressibility
CS	Carbon steel
Dev	Deviation
DBDP	Difference between bubble point and dew point
DP	Dew point
ECV	Effective CO_2 volume
EOR	Enhanced oil recovery
EOS	Equation of state
Equ.	Equation
EvGT	Evaporative gas turbine
FCT	Flue gas condensing temperature
FP	Flat plate
GHG	Green house gases
HAT	Humid air turbine
IGCC	Integrated gasification combined cycle

IPCC	Intergovernmental Panel on Climate Change
ISRK	Improved Soave-Redlich-Kwong
LHV	Lower heating value
MEA	Mono-methyl ethanolamine
MPR	Modified Peng-Robinson
MSRK	Modified Soave-Redlich-Kwong
O&M	Operation and maintenance
PR	Peng-Robinson
PSRK	Predictive- Redlich-Kwong-Soave
PT	Patel-Teja
PUR	Purification
RK	Redlich-Kwong
SRK	Soave-Redlich-Kwong
SS	Stainless steel
STIG	Steam injection gas turbine
STP	Stripper pressure
TEG	Triethylene glycol
TET	Turbine exit temperature
TIT	Turbine inlet temperature
TRA	Transport
T-S	Tube-shell
VLE	Vapour liquid equilibrium
W/A	Water/Air ratio

Subscript:

c	Critical
cal	Calculated
exp	Experimental
g	Gas
i, j	Component labels
l	Liquid
s	Saturated
0	Reference status

1 Introduction

1.1 Global Warming and CO_2 Capture and Storage (CCS)

Emissions of greenhouse gases (GHG) have been associated with a rise in the global average temperature. The global average temperature has been increased by 0.74K since the late 1800s and, according to the Intergovernmental Panel on Climate Change (IPCC), is expected to further increase by another 1.1 to 6.4K by the end of 21st century [1]. A global warming may lead to serious consequences. For example, the average sea level has risen by 10 to 20cm during the past century, and an additional increase of 9 to 88cm is expected by the year 2100 [2]. Therefore, IPCC has stated that global GHG emissions should be reduced by 50 to 80 percent by the year 2050 [3].

The largest contributor amongst the greenhouse gases is carbon dioxide (CO_2), which is released by burning such fossil fuels as coal, oil and natural gas, and by the burning of forests. Carbon dioxide capture and storage (CCS), which involves the capture, transport and long-term storage of carbon dioxide, is a technically feasible method of making substantial reductions of CO_2 emissions. CCS is a critical technology amongst a portfolio of measures to limit climate change to a manageable level, along with improving the efficiency of energy conversion and/or utilization, and switching to renewable energy resources. The importance of CCS has been highlighted in Figure 1.1 as one of the key elements in the strategy of reducing greenhouse gas emissions [4]. At present, the main application for CCS is in power generation systems [5].

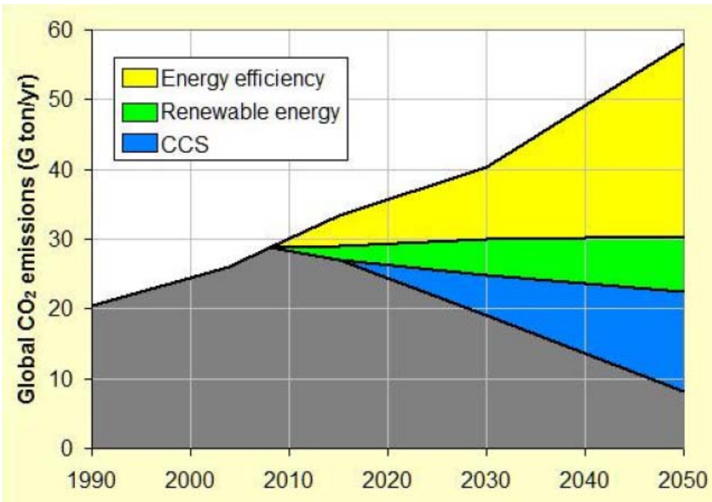

Figure 1.1 Strategy to reduce global CO_2 emissions [4]

As shown in Figure 1.2, there are three main technology options for CO_2 separation from power plants: post-combustion capture, pre-combustion capture, and oxy-fuel combustion capture. Post-combustion capture means capturing CO_2 from the flue gases produced by the combustion of fossil fuels and biomass in air. It is a downstream process, in which the CO_2 in flue gas at near atmospheric pressure is typically removed by a chemical absorption process using absorbents such as *alkanolamines*. Pre-combustion capture is to separate the fuel-bound carbon before the fuel is combusted. This involves a reaction between fuel and oxygen to primarily give a '*synthesis gas*' or '*fuel gas*', which contains carbon monoxide and hydrogen. The carbon monoxide reacts with steam in a catalytic reactor, called a shift converter, to give CO_2 and more hydrogen. CO_2 is then separated, usually by a physical or chemical absorption process. Oxy-fuel combustion capture means capturing CO_2 from the flue gases produced in oxy-fuel combustion. The oxy-fuel combustion is the combustion taking place in a denitrogenation environment, resulting in a flue gas mainly consisting of H_2O and CO_2. The technical-economic comparison of the three CO_2 capture technologies is still under way especially for large-scale industrial applications. A preferable technology may highly depend on its further development and commercialization of the technologies.

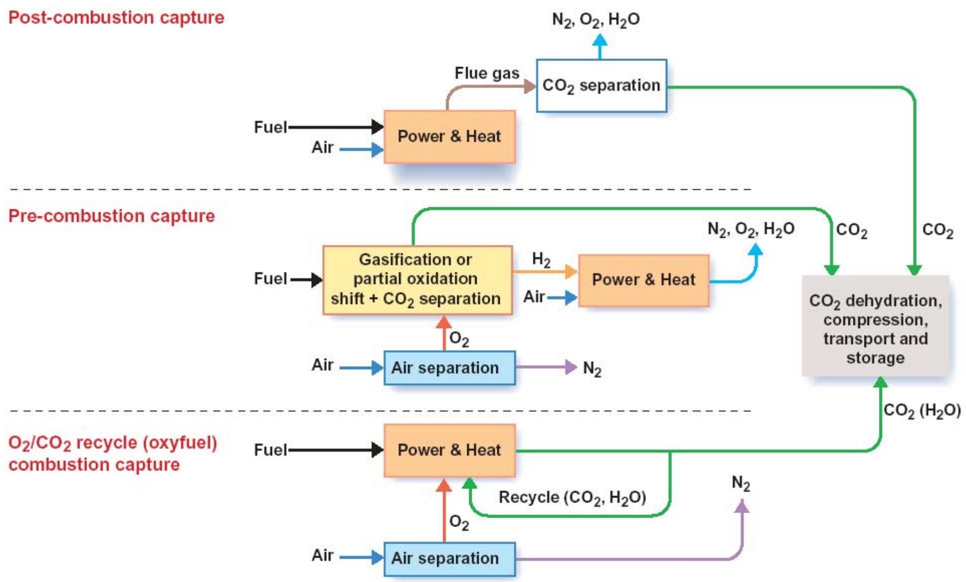

Figure 1.2 Basic principles of three CO_2 capture technologies for fossil fuel power generation

1.2 Problems and Challenges

The thermodynamic properties of CO_2 mixtures are essential for the design and operation of the CCS systems. How a specific operation parameter affects the performance and costs of the CO_2 capture system highly depends upon the knowledge of thermodynamic properties of CO_2 mixtures. For example, the vapour-liquid equilibrium (VLE) of CO_2 mixtures is the basic parameters to design necessary purification processes for CO_2 mixtures captured from the flue gas of coal-fired power generation. Meanwhile, for CO_2 transportation, it is preferable to transport CO_2 in a high-density state and avoid the occurrence of two-phase flow in order to reduce the energy consumption and investment costs, and to secure operation safety. In order to guarantee the right operation conditions, the accurate thermodynamic properties of CO_2 mixtures are of great importance to control and adjust parameters for the CCS system operation.

Therefore, a better understanding of the thermodynamic properties of CO_2 mixtures could provide a scientific basis to define a proper guideline of CO_2 purity and impure components for the CCS processes according to technical, safety and environmental requirements. The more knowledge of the thermodynamic properties, the more accurate, more economic, and safer guidelines of CO_2 purity could be defined. Moreover, new CO_2 capture system development and technical breakthrough will also rely upon a deeper understanding of the thermodynamic properties of CO_2 mixtures and the related impurities. The existence of impurities, however, makes it more difficult.

The most precise way to study the thermodynamic properties of CO_2 mixtures is via experiments. However, there are some critical issues regarding experimental data. Those CCS processes cover a large range of operation conditions from normal atmosphere to supercritical state, and involve multi-component mixtures; therefore, the limited experimental data cannot satisfy the requirements of the engineering applications.

In order to break the limitations of experiments, theoretical mathematic models are usually used to predict thermodynamic properties. Due to the rapidly developing research on CCS, there has been an increasing interest in finding proper theoretical models to predict the thermodynamic properties of CO_2 mixtures. So far, there are many available models of various types. It has been proven that the reliabilities of models vary for different properties, components and conditions [6-8]. However, only a little work has been done regarding several CO_2 mixtures; and no comprehensive evaluations and recommendations are addressed concerning the applications in the CCS systems. For example, Carroll only studied Peng-Robinson (PR) [9] and Redlich-Kwong-Soave (SRK) equations of state (EOS) [10] for the VLE calculations of the binary CO_2 mixtures including CH_4 and H_2S [11-12].

1.3 Objectives

One of the main objectives of this thesis is to study the thermodynamic properties of CO_2 mixtures and analyze their impacts on the processes of CCS. In order to properly conduct the work, it is necessary to find or develop the proper models for the thermodynamic property calculation.

Another important objective is to have an overview of the advanced power cycles combined with different CO_2 capture technologies, from both technical and economic aspects, by applying the results, obtained from the property study, in the system simulations. A novel gas turbine cycle, evaporative gas turbine cycle (EvGT), was investigated as it is integrated with chemical absorption capture and oxy-fuel combustion capture.

1.4 Methodology

Figure 1.3 illustrates the flow chart of this study. The required thermodynamic properties and operation conditions of CCS were first identified in order to make the study more specific; then the available experimental data on the thermodynamic properties of CO_2 mixtures were collected. Based upon the data, different theoretical models were evaluated and the recommendations of calculation methods were provided regarding the engineering design of CCS systems. With the determined appropriate methods, the impacts of impurities upon the thermodynamic properties of CO_2 mixtures and the performances of different processes involved in CCS were investigated. The results would be helpful to the design and optimization of the power cycles combined with different CO_2 capture technologies.

In this study, our self-programming codes are used to conduct the calculations about the thermodynamic property and investigate the impacts of impurities on some processes involved in CCS, such as compression and flash purification; while the humid gas turbine cycles integrated with CO_2 capture are simulated with Aspen Plus.

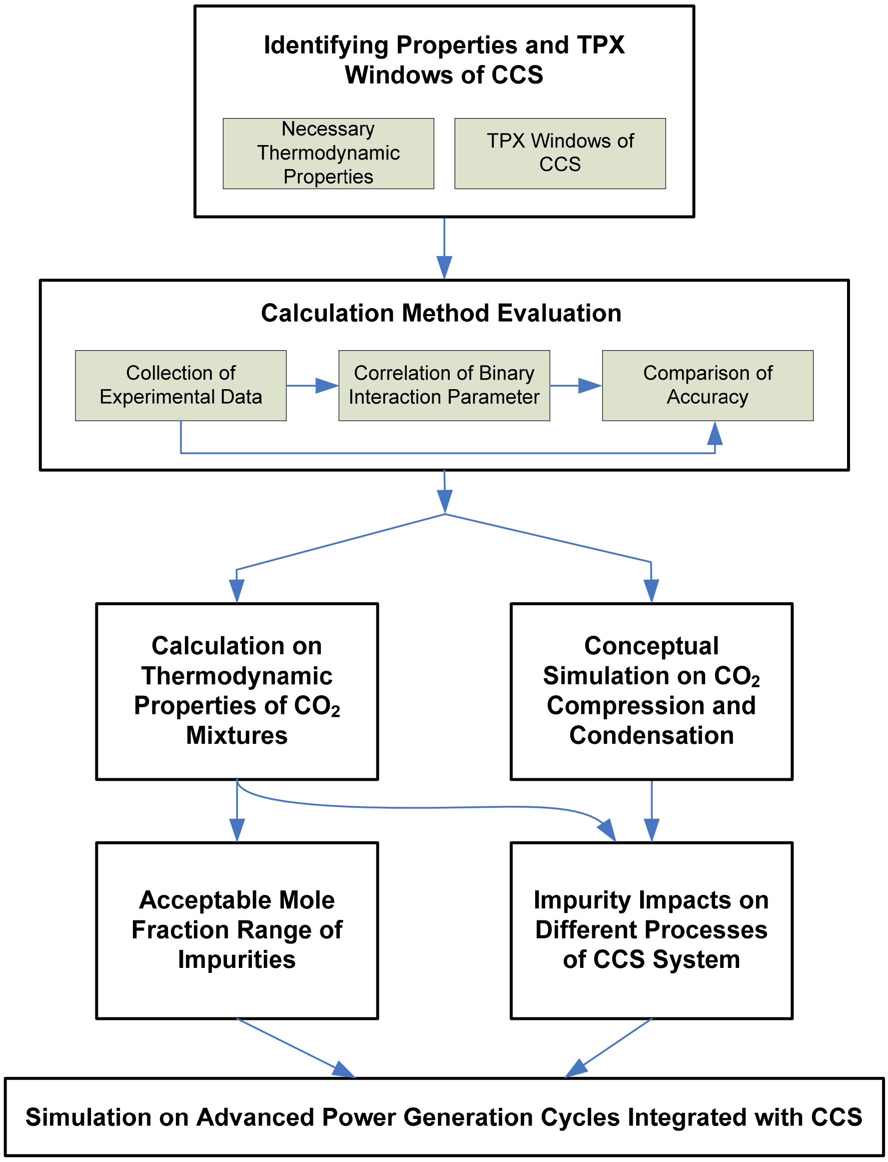

Figure 1.3 Flow chart of this study

1.5 Outline of the Thesis

The thesis is a summary of eight scientific papers, which are appended, and two technical reports. The research can be divided into two parts: Thermodynamic Properties of CO_2 Mixtures, which includes Chapter 2 and 3; and Evaporative Gas Turbine Cycles Integrated with CO_2 capture, which includes Chapter 4.

Chapter 2 investigates the calculation methods about the thermodynamic properties of CO_2 mixtures. Section 2.1 summarizes the required thermodynamic properties, the possible operation conditions, such as temperature and pressure windows for different the CCS processes, and the potential impurities. In Section 2.2, experimental data are collected concerning those required properties, and the experimental data gap is identified for the method evaluations. In Section 2.3, various theoretical models on the thermodynamic property calculation are evaluated based upon the collected experimental data. Finally suggestions on method selection are provided in Section 2.4. The presented material is based upon Papers I, V and VIII and Report I

Chapter 3 investigates the impacts of impurities upon the thermodynamic properties of CO_2 mixtures and the different processes involved in the CCS systems. It has been identified that impurities affect the CCS processes through their impacts upon the thermodynamic properties of CO_2 mixtures. The basic material is taken from Papers II - IV and Report II.

Chapter 4 addresses the study of the advanced power cycles combined with CO_2 capture processes. Section 4.1 introduces three system configurations including EvGT, EvGT + Chemical Absorption CO_2 Capture, and EvGT + Oxy-fuel Combustion. In Section 4.2 and 4.3, those systems are analyzed from the view points of both thermodynamic efficiency and investment cost respectively. In Section 4.4, several issues regarding the electrical efficiency are investigated. Results given in this chapter are based upon Paper VI and VII.

Chapter 5 summarizes the conclusions found during the course of this research.

Part I: Thermodynamic Properties of CO_2 Mixtures

2 Method Evaluations for the Thermodynamic Property Calculations of CO_2 Mixtures

2.1 Necessary Thermodynamic Properties and Potential Operation Conditions of CCS

2.1.1 Required Thermodynamic Properties and Their Relation to Engineering Design

The major thermodynamic properties of CO_2 mixtures required by the design of the CCS systems have been identified based upon main processes and corresponding components as shown in Table 2.1 [13]. Meanwhile VLE and volume are the basis for other property calculations. Therefore VLE and volume are considered to be the most important properties in this study.

Table 2.1 Major thermodynamic properties of CO_2 mixtures required by the CCS system design and engineering evaluation

	Thermodynamic properties			
	Phase equilibrium	Volume	Enthalpy	Entropy
Capture				
Compression	√	√	√	√
Purification	√	√	√	√
Refrigeration	√		√	√
Transportation				
Pipeline	√	√	√	√
Small tanks	√	√	√	√
Large tanks	√	√	√	√
Storage				
Injection	√	√	√	√
Storage	√	√		

2.1.2 Operating Windows of the CCS Processes

In order to determine the data needs for the evaluation of CO_2 thermodynamic properties in the CCS processes, the operating window should be defined with the regions of phases and the CCS processes. The operation conditions of the temperatures and pressures provide the basis upon which to identify the relevant experimental data requirements and applied range, in which property models should preferably be used to minimize the uncertainties.

A typical CCS procedure from a fossil fuel power generation normally consists of four steps: CO_2 capture from flue gas, CO_2 processing (compression, dehydration, purification/liquefaction, and further compression/pumping), CO_2 transport and CO_2 storage. The four steps make up a process chain for CCS. The operation conditions of the CCS processes are estimated in terms of pressure and temperature in Table 2.2 [13]. Some sub-processes or options for these CCS processes are indicated in Table 2.2 as well. The P-T windows are illustrated in Figure 2.1, mainly based on the estimated operation conditions of the CCS processes.

Table 2.2 Estimated operation conditions (P and T) of the CCS processes

CCS process	P (MPa)	T (K)
CO_2 compression/purification	*0 to 11*	*219.15 to 423.15*
Initial compression	0 to 3	293.15 to 423.15
Dehydration	2 to 3	283.15 to 303.15
Purification	2 to 5	219.15 to 248.15
Further compression/pumping	5 to 11	283.15 to 303.15
CO_2 transport	*0.5 to 20*	*218.15 to 303.15*
Pipeline	7.5 to 20	273.15 to 303.15
Small tanks	1.5 to 2.5	238.15 to 248.15
Large tanks	0.5 to 0.9	218.15 to 228.15
CO_2 storage	*0.1 to 50*	*277.15 to 423.15*

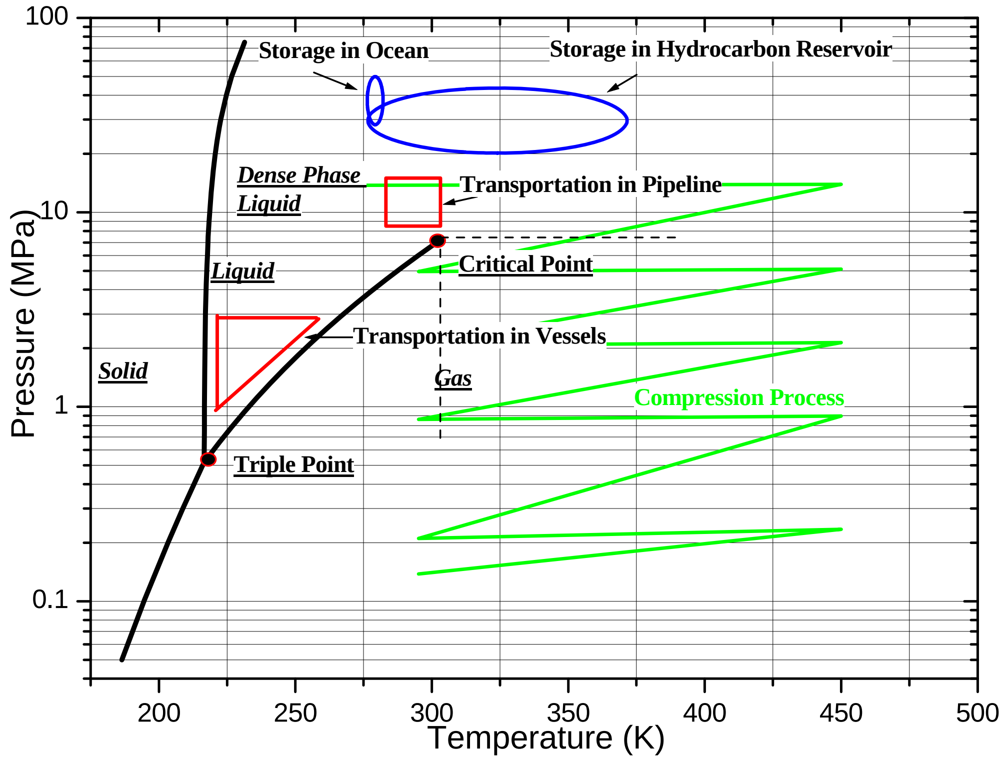

Figure 2.1 Potential pressure and temperature windows of the CCS systems

2.1.3 Impurities in CO_2 Mixtures

Generally there are no strong technical barriers to provide high purity of CO_2 from the flue gas of fossil fuel fired power plants. However, high purity requirements are likely to induce additional costs and energy requirements resulting in a loss of power plant efficiency. It is of importance to find an optimal balance amongst the requirements from purification, transport, storage, legal and environmental aspects.

The characteristics of the CO_2 streams captured from the power generation may vary depending on the CO_2 capture technology used for CCS. The CO_2 streams captured from post-combustion with an amine solution is relatively clean. H_2O is the main impurity. However, relative high levels of impure components are expected in the captured CO_2 streams from oxy-fuel combustion, and a more complicated composition of the CO_2 streams is found in the Integrated Gasification Combined Cycle (IGCC) cases, mainly including different hydrocarbons, such as CH_4.

Based on the fuel conversion processes for power generation and the speciation of major impurities, the captured CO_2 streams could be categorised into two types [14]:

- Oxidising CO_2 streams with residual O_2 and contaminated sulphur components mainly with SO_2 (e. g. CO_2 captured from oxy-fuel and post combustions); and,
- Reducing CO_2 streams with almost no residual O_2 and contaminated sulphur components mainly with H_2S (e. g. CO_2 captured from coal gasification processes such as IGCC).

The major differences of the two types of captured CO_2 streams are the concentrations of non-condensable impurities such as N_2, Ar, and O_2 and types of impurities due to the different redox conditions in the CO_2 streams, for example the oxidising sulphur species SO_2 existing in oxidising CO_2 streams while the reducing species H_2S existing in reducing CO_2 streams. Therefore, the impurities, including N_2, O_2, Ar, H_2O, CH_4, SO_2, and H_2S, are considered for the study of the thermodynamic properties of their CO_2 mixtures in this research, which may cover the most interest non-CO_2 components existing in the captured CO_2 streams.

2.2 Available Experimental Data and Gaps Regarding CO_2 and CO_2 Mixtures

Accurate experimental data of both pure CO_2 and CO_2 mixtures (CO_2 + impurities) are required to verify the reliabilities of calculation models and calibrate parameters contained in the models.

Since the 1980s, many experiments with higher accuracy have been conducted for pure CO_2 properties. For the thermodynamic properties of CO_2 mixtures, investigations were also carried out but focused mainly on the impurities, such as water, hydrocarbons, nitrogen, and hydrogen sulphide due to their importance for production and processing of natural gas resources and for using the CO_2 mixture for enhanced oil recovery (EOR) process. As a result, there are a lot of available experimental data about the mixtures of CO_2/H_2O, CO_2/N_2, CO_2/CH_4, and CO_2/H_2S, which cover a wide range of temperature and pressure. However, the experimental data of the CO_2 mixtures containing O_2, Ar, and SO_2 are limited, although such impurities in CO_2 are important for the CCS processes, especially the oxy-fuel combustion technology.

Available experimental data of pure CO_2 are summarized in Table 2.3. Different kinds of properties including volume, C_p, VLE, and excess enthalpy are included.

Table 2.3 Summary of the available experimental data for pure CO_2

Source	Year	Type	T (K)	P (MPa)	Uncertainty
Holste et al [15]	1987	Volume	215-448	0.1-50.0	P: ±0.01%; T: ±0.01K;
Ernst et al [16]	1989	C_p	303.15-393.15	0.1-90	-
Duschek [17]	1990	VLE	217-340	0.3-9.0	P: ±0.02%; T: ±0.003K[a]
Gilgen et al [18]	1992	Volume	220-360	0.3-13.0	V:±(0.015~0.04)%
Brachthuser [19]	1993	Volume	233-523	0.8-30.1	V: ±(0.02~0.04)%
Möller et al [20]	1993	Excess Enthalpy	230-350	15-18	-
Fenghour [21]	1995	Volume	329.82-697.81	3.032-34.203	P: ±0.02%; T: ±0.01K;
Klimeck et al [22]	2001	Volume	240-470	0.5-30	P: ±0.016%' T: ±0.004K[b];

Available experimental data of the CO_2 mixtures containing those impurities (N_2, O_2, Ar, SO_2, CH_4, H_2O and H_2S) are summarized in Table 2.4. They are mainly about the properties of VLE and volume. Meanwhile almost all of them are about binary CO_2 mixtures.

Table 2.4 Summary of the experimental data for binary CO_2 mixtures

Source	Year	Type	Mixture	T (K)	P (MPa)	Uncertainty
Caubet [23]	1901	TPVX	CO_2/SO_2	291-416	2.7-10.5	
Reamer et al [24]	1944	TPxy	CO_2/CH_4	311-511	1.4-69	
Steckel [25]	1945	PTxy	CO_2/H_2S	221-288.15	0.1-3.6	
Bierlein et al [26]	1953	PTVX	CO_2/H_2S	273-370	1.5-8.5	V: ±0.02% T: ±0.02K
Donnelly et al [27]	1954	TPxy	CO_2/CH_4	167-301	2.0-7.4	
Muirbrook et al [28, 29]	1965	TPxy	CO_2/O_2, CO_2/N_2, $CO_2/N_2/O_2$	273.15	5.5-12	P: ±0.1%
Kestin et al [30]	1966	TPVX	CO_2/Ar	293.15-303.15	0.101-2.58	P: ±0.5% * T: ±1K
Greenwood [31]	1969	TPxy	CO_2/H_2O	723-1073	Up to 50	
Fredenslund et al [32]	1970	TPxy	CO_2/O_2	223.15-283.15	1-13	P: ±0.5% T: ±0.02K
Arai et al [33]	1971	PVTx	CO_2/N_2, CO_2/CH_4	253-288	5-15	P: ±0.01atm T: ±0.01K
Sarashina et al [34]	1971	PVTx	CO_2/Ar	288.15	5.69-9.77	P: ±0.01atm T: ±0.01K
Davalos et al [35]	1976	PTxy	CO_2/CH_4	230-250	0.9-8.5	
Altunin et al [36]	1977	Comp	CO_2/Ar	303.15	0.29-10.75	
Mraw et al [37]	1978	TPxy	CO_2/CH_4	89-208	0.5-6.3	
Somait et al [38]	1978	TPxy	CO_2/N_2	270	3-12	P: ±0.015atm T: ±0.02K
Zawisza and Malesinska [39]	1981	TPVX	CO_2/H_2O	323-473	Up to 3.3	P: ±0.03% T: ±0.05K
Dorau et al [40]	1983	TPxy	CO_2/N_2	223.15-273.15	3-20	
Patel and Eubank [41]	1988	TPVX	CO_2/H_2O	323-498	Up to 10.34	P: ±0.01%; T: ±0.01K
Esper et al [42]	1989	TPVX	CO_2/N_2	205-320	0.1-48	P: ±0.015% T: ±0.01K
Sterner and Bodnar [43]	1991	TPVX	CO_2/H_2O	673-973	200-600	P: ±1% T: ±1% °C
Fenghour [44]	1994	TPVX	CO_2/H_2O	415-700	6-35	P: ±0.02% T: ±0.01K
Seitz and Blencoe [45]	1999	TPVX	CO_2/H_2O	673	10-100	P: ±0.01MPa T: ±0.01K

* If partial pressure of CO_2 was less than 5MPa, uncertainty was 1.5 percent.

Tables 2.5 and 2.6 summarized the ranges of T, P, x and y of the experimental data on VLE and volume. There are still some gaps between available experimental data and requirements of method for the evaluation and calibration. For example, there are few experimental data on VLE of CO_2/SO_2 at temperatures below 290K; there are few experimental data on VLE of CO_2/Ar, except at the temperature of 288.15K and pressure 5~10MPa; and there are no experimental data on volume of CO_2/O_2. Moreover only a few of the experimental data are available for multi-component CO_2 mixtures such $CO_2/N_2/O_2$.

Table 2.5 Summary of TPxy ranges of the VLE experimental data for binary CO_2 mixtures

	T (K)	P (MPa)	x_{CO2}	y_{CO2}	No. of Exp. Point
CO_2	216.58-303.90	0.52-7.32	-	-	27
CO_2/O_2	223.15-283.15	1.01-12.16	0.62-0.999	0.18-0.91	72
CO_2/N_2	253.15-288.15	2.35-13.95	0.43-1.00	0.43-1.00	67
CO_2/SO_2	295.15-338.45	2.12-6.43	-	0.75-0.93	91
CO_2/H_2S	255.15-363.15	2.03-8.11	0.01-0.97	0.05-0.97	77
CO_2/Ar	288.15	5.69-8.38	0.83-0.94	0.79-0.94	10
CO_2/CH_4	193.15-270	0.68-8.41	0.026-0.99	0.026-0.917	82
CO_2/H_2O	276.15-642.7	Up to 310	0~0.99	0~0.99	>1000

Table 2.6 Summary of TPxy ranges of the volume experimental data for binary CO_2 mixtures

	Phase	T (K)	P (MPa)	x_{CO2}	y_{CO2}	No. of Exp. Point
CO_2		215.00-697.81	0.30-50.00			>1000
CO_2/O_2	V_g	NA				
	V_l	NA				
CO_2/N_2	V_g	253.15-288.15	2.35-14.51		0.49-1	120
	V_l	253.15-288.15	2.43-14.51	0.85-1		64
CO_2/SO_2	V_g	287.15-347.35	0.10-7.60		0.125-0.927	120
	V_l	299.15-341.15	5.67-10.64	0.125-0.927		36
CO_2/H_2S	V_g	278.05-304.86	3.50-6.99		0.83-0.90	16
	V_l	275.07-306.27	3.50-6.99	0.83-0.90		16
CO_2/Ar	V_g	293.15-303.15	0.10-2.50		0.84-0.92	16
	V_l	288.15	7.51-9.78	0.83-0.94		4
CO_2/CH_4	V_g	219.7-300	0.1-14.3		0.45-0.96	245
	V_l	273-293	6-14	0.56-0.96		47
CO_2/H_2O	V_g	323-1073	Up to 600		0.-0.99	>2000
	V_l	278-471	0-31	0-0.99		>300

2.3 Evaluation of Calculation Models on Thermodynamic Properties of CO_2 Mixtures

2.3.1 Introduction of the Calculation Models

The correlation and prediction of mixture behaviours are one of the central topics in applied thermodynamics. There are generally two types of thermodynamic methods for phase equilibrium calculations: liquid activity coefficient based models and equation-of-state based models. Activity coefficient models are the best way to represent highly non-ideal liquid mixtures at low pressures, and can be used to describe mixtures of any complexity. The equation of state methods can be applied over wide ranges of temperature and pressure, including sub-critical and super-critical regions. For ideal or slightly non-ideal systems, the thermodynamic properties for both the vapour and liquid phases can be computed with a minimum amount of component data. However, the EOS method has relatively poor accuracy for liquid phase calculations. Considering the wide range of operation conditions of the CCS processes and many required thermodynamic properties, EOS may be more applicable than activity coefficient methods, because activity coefficient method can only be used in low pressure cases (usually those lower than 10atm) [47] and has more complicated procedure to calculate other thermodynamic properties, such as volume, enthalpy, and entropy.

A semi-empirical EOS relates volume, pressure, temperature and composition of substances in mathematical forms [46]. Any thermodynamic property can be obtained from it by using appropriate thermodynamic relations [48]. However, the development of such semi-empirical equations requires a great deal of experimental data on wide range to the corresponding substance. The shortage of those experimental data makes the progress slow and limited to a few pure fluids nowadays.

EOS can be divided into two categories: specialized EOS, such as Span's EOS [49] for CO_2, and general EOS, such as van der Waals EOS [50]. Compared with the latter, specialized equations have a better accuracy; however, their applications are limited to certain substances. For example, Span's EOS can only be applied to CO_2. Meanwhile the general equations can be further divided into two types: equations with simple structures, such as Redlich-Kwong (RK) EOS [51]; and equations with complex structures, such as Benedict-Webb-Rubin (BWR) EOS [52]. Although the general equations with complex structure may give better results, as they contain more parameters, their calculation procedures on the thermodynamic properties are more complicated, especially when calculating some derived properties such as enthalpy and entropy. In addition, also due to the complicated calculation procedure, it is more difficult to integrate the general equations with complex structure into some commercial software, such as Aspen Plus [47] and IPSpro [53], if they are not originally included.

Thus, from an engineering standpoint, a general EOS with simple structure and reasonable accuracy is more preferable. Cubic equations of state have very simple structures. Since van der Waals proposed his EOS in 1873, numerous modified versions of cubic EOS with two or more parameters have been developed to improve predictions of volumetric and phase equilibrium properties of fluids. It has been well established that a cubic EOS can satisfactorily model phase equilibrium. In this work, RK was modified for gaseous CO_2 and gaseous mixtures of CO_2/H_2O; moreover the reliabilities of cubic equations of state were evaluated for predicting the thermodynamic properties of CO_2 mixtures.

2.3.2 A New Model for Gaseous CO_2 and Gaseous Mixtures of CO_2/H_2O

Since the 1980s, new experiments on gaseous CO_2 and gaseous mixtures of CO_2/H_2O have been conducted. However, little work on equation of state has been done regarding the requirements of engineering applications. Under such a situation, a new correlation was developed with the consideration of new experimental data.

It has been verified that RK EOS [50] can represent vapour and liquid behaviours effectively. It was proposed in 1949 as:

$$P = \frac{RT}{v-b} - \frac{a}{v(v+b)T^{1/2}} \tag{2.1}$$

Where 'a' and 'b' are parameters. Parameter 'a' reflects intermolecular attraction, and parameters 'b' reflects molecular size (repulsive forces). For simple non-polar gases, they can be calculated from critical data.

$$a = \frac{0.42748 R^2 T_c^{2.5}}{P_c}$$
$$b = \frac{0.08664 R T_c}{P_c} \tag{2.2}$$

According to Bottinga's conclusions [54], if the parameters 'a' and 'b' were expressed by functions, RK EOS can describe properties more accurately, even for polar gases. Therefore, in the current research, and based upon more precisely measured PVTs properties, RK EOS will be modified for better precision for gaseous CO_2 and for larger application range for gaseous mixtures of CO_2 and H_2O. New description of parameter 'a' for gaseous CO_2 is given in Equ. 2.3.

$$a = a_1 + a_2 P$$
$$a_1 = \frac{2.3457 \times 10^5}{T^2} - \frac{1.3612 \times 10^3}{T} - 4.8365 \times 10^{-3} T + 9.9191$$
$$a_2 = \frac{1.9141 \times 10^{-2}}{T^2} - \frac{1.0132 \times 10^{-4}}{T} - 1.3654 \times 10^{-10} T + 0.1934 \times 10^{-6} \tag{2.3}$$
$$b = \frac{0.08664 R T_c}{P_c}$$

For gaseous CO_2/H_2O, we modified the mixing rules:

$$a = \sum_i \sum_j y_i \cdot y_j \cdot a_{ij} \tag{2.4}$$

$$b = \sum_i y_i \cdot b_i \tag{2.5}$$

With

$$a_{ij} = a_{ji} = 40.1248 + 4.5108 \times 10^{-7} \cdot T^{2.5} \cdot e^{\frac{1.6060 \times 10^3}{T} - \frac{4.9003 \times 10^5}{T^2} + \frac{1.4556 \times 10^8}{T^3}} \tag{2.6}$$

Compared with experimental data, the absolute average deviation (AAD), which is defined as:

$$AAD = \frac{\sum abs\left(\frac{M_{cal} - M_{exp}}{M_{exp}}\right) \times 100\%}{N} \tag{2.7}$$

of the new model is 1.68% for the volume of gaseous CO_2 in the range 220-700K and 0.1-400MPa except for the critical region (295-315K and 6.5-9.5MPa); and 0.93% for the volume of gaseous CO_2/H_2O in the range 323-1073K and 0.1-600MPa. Calculated results on other thermodynamic properties, such as enthalpy and heat capacity, also fit the experimental data well. More detailed results were summarized in Paper I.

2.3.3 Evaluations of Cubic EOS for Predicting VLE and Volume of CO_2 mixtures

2.3.3.1 Prediction of VLE

Five cubic EOS widely used in the petroleum and gas industries are evaluated for the calculation on VLE properties, including Peng-Robinson (PR) [9], Patel-Teja (PT) [55], Redlich-Kwong (RK), Redlich-Kwong-Soave (SRK) [56], and 3P1T [57]. All studied equations of state are summarized in Table 2.7 with the features as described below:

- PR EOS is proposed based upon RK EOS. It is capable of predicting the liquid volume as well as vapour pressure in order to further improve VLE predictions. It is recommended for hydrocarbon processing applications, such as gas processing, refinery, and petrochemical processes.
- PT EOS has two substance dependent parameters which are obtained from the liquid volume and vapour pressure data, and correlated with an acentric factor. The 3-parameter PT equation has been shown to give satisfactory results for both vapour pressure and volume even for heavy and polar compounds. It is also recommended for hydrocarbon processing applications.
- RK EOS is the earliest modification of van der Waals EOS; it improved the intermolecular attraction. It is more applicable for the system at low pressures.
- SKR EOS is another modification of RK EOS by introducing a temperature-dependent function to modify the attraction parameter. It was one of the most popular EOS in the hydrocarbon industry. SRK is capable of predicting VLE for liquid mixtures; however, it is not very satisfactory for predictions of liquid compressibility.
- 3P1T EOS is an equation of van der Waals type. It was primarily developed for non-polar compounds, however, it was claimed to be able to be applied for polar substances as well [57].

The semi-empirical equations of state have been developed by using pure component data. The application of these equations has been extended to a multi-component system by defining mixing rules to evaluate the average parameters required in the calculations. In this study, the conventional random van der Waals mixing rules were employed for all of EOS. In the mixing rules, there is one very important parameter, binary interaction parameter k_{ij}, which accounts for the attraction forces between pairs of non-similar molecules. Theoretically, it is a modification of intermolecular attraction when calculating thermodynamic properties of mixtures. The value of k_{ij} is more sensitive to derivative or partial properties such as fugacity coefficients than to total properties such as mixture molar volumes. For that reason, values of k_{ij} have most often been determined from VLE data.

Since the determination of k_{ij} requires a large amount of experimental data, the calibrated binary interaction parameters are not known for all the binary systems and EOS. If the calibrated k_{ij} is unknown, for approximate calculation the difference of attraction forces, which are between non-similar molecules and between similar molecules, can be ignored, and different molecules can be regarded as same. Thus, values of k_{ij} would be taken as zero (if $(1-k_{ij})$ is used in the mixing rules, such as RK EOS) or unity (if (k_{ij}) is used in the mixing rules, such as PT EOS).

Table 2.7 Summary of studied cubic EOS for VLE calculations

EOS	Function Form	Mixing Rule
PR	$P=\frac{RT}{V-b}-\frac{a}{V(V+b)+b(V-b)}$	$a=\sum_i\sum_j x_i x_j a_i^{1/2} a_j^{1/2}(1-k_{ij})$; $b=\sum_i x_i b_i$; $k_{ij}=k_{ji}$;
PT	$P=\frac{RT}{V-b}-\frac{a(T)}{V(V+b)+c(V-b)}$	$a=\sum_i\sum_j x_i x_j a_i^{1/2} a_j^{1/2}\xi_{ij}$; $b=\sum_i x_i b_i$; $c=\sum_i x_i c_i$; $\xi_{ij}=\xi_{ji}$
RK	$P=\frac{RT}{V-b}-\frac{a/T^{0.5}}{V(V+b)}$	$a=\sum_i\sum_j x_i x_j a_i^{1/2} a_j^{1/2}(1-k_{ij})$; $b=\sum_i x_i b_i$; $k_{ij}=k_{ji}$
SRK	$P=\frac{RT}{V+c-b}-\frac{a}{(V+c)(V+b+c)}$	$a=\sum_i\sum_j x_i x_j a_i^{1/2} a_j^{1/2}(1-k_{ij})$; $b=\sum_i x_i b_i$; $c=\sum_i x_i c_i$; $k_{ij}=k_{ji}$
3P1T	$P=\frac{RT}{V-b}-\frac{a}{V^2+ubV+wb^2}$	$a=\sum_i\sum_j x_i x_j a_i^{1/2} a_j^{1/2}(1-k_{ij})$; $b=\sum_i x_i b_i$; $k_{ij}=k_{ji}$

However, an inappropriate k_{ij} may cause a poor calculating accuracy of an EOS. Figure 2.2 shows the sum of average absolute deviation (AAD), on the saturated pressure and AAD on the saturated vapour fraction of CO_2 ($y_{s,CO2}$) at different binary interaction parameter k_{ij}, (to PT EOS, it is $(1-k_{ij})$). It is clear that AAD changes with the variation of k_{ij}.

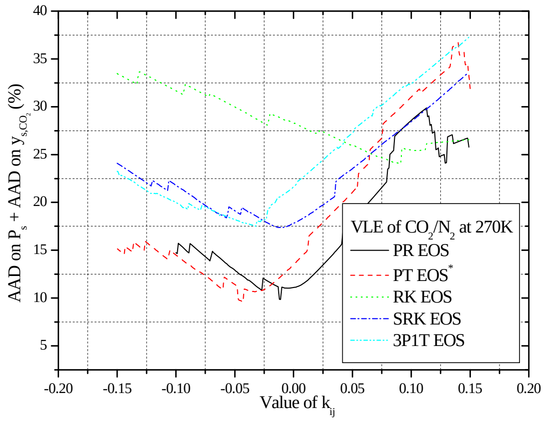

Figure 2.2 Relationship between calculation accuracy and binary interaction parameter

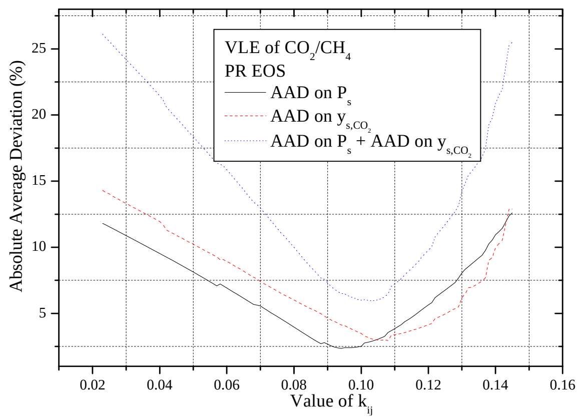

Figure 2.3 AAD on P_s, $y_{s,CO2}$, and $P_s+y_{s,CO2}$ of CO_2/CH_4 at different k_{ij}

In order to improve the accuracy of cubic equations and evaluate EOS precisely, the binary interaction parameters of various binary CO_2 mixtures must first be determined. Usually, the binary interaction parameter k_{ij} is considered to be independent of temperature, composition, and volume [58]. However, there are also some different conclusions that k_{ij} is temperature and composition dependent [59-61]. As k_{ij} is determined by matching the predicted values with experimental data, it should be considered as a fitting parameter only and not a rigorous physical parameter [7]. Hence, in this study, the value of k_{ij} is still regarded as a constant.

The saturated pressures and saturated vapour compositions have been calculated from the known saturated temperatures (T_s) and saturated liquid compositions (x_s). Figure 2.3 shows the AAD of PR EOS on P_s, $y_{s,CO2}$, and P_s+$y_{s,CO2}$ of CO_2/CH_4 at different k_{ij}. This clearly displays that for various properties, the binary interaction parameter may be calibrated as different values. Since both saturated pressure and saturated vapour composition are important to the CCS processes, here k_{ij} is calibrated as the value that makes the sum of AAD on P_s and $y_{s,CO2}$ minimum (For CO_2/Ar and CO_2/SO_2. because x_s and y_s are not known at dew points and bubble points, respectively, no AAD on $y_{s,CO2}/x_{s,CO2}$ are calculated. In these cases, the value of k_{ij} that makes the AAD on P_s minimum is chosen.). The flow chart of the procedure for regressing k_{ij} is shown in Appendix A. Based upon the experimental data listed in Table 2.4, k_{ij} was calibrated for each EOS concerning each binary mixture. Since CO_2/H_2O has been examined intensively in previous studies [62, 63], here H_2O is excluded. Results are given in Table 2.8.

Table 2.8 Correlated k_{ij} for different binary CO_2 mixtures based on VLE experimental data

	PR	PT	RK	SRK	3P1T
CO_2/CH_4	0.103	0.903	0.084	0.104	-0.050
CO_2/O_2	0.115	0.898	0.178	0.118	0.105
CO_2/H_2S	0.099	0.907	0.083	0.106	0.098
CO_2/N_2	-0.011	1.043	0.089	-0.011	-0.032
CO_2/Ar	0.228	0.806	-0.084	0.224	-0.128
CO_2/SO_2	0.047	0.953	-0.041	0.048	0.083

With the new calibrated k_{ij}, VLE of different binary CO_2 mixtures were calculated using different EOS; and the calculated results were compared with experimental data. Table 2.9 summarizes the absolute average deviations of EOS. All of the studied EOS have various performances for various mixtures; and comparatively PR, PT and SRK are superior to RK and 3P1T for all of the studied mixtures. It should be stressed that although 3P1T is primarily developed for non-polar compounds, it doesn't show any advantages in the VLE calculations of CO_2/CH_4, CO_2/O_2, CO_2/N_2, and CO_2/Ar. For detailed analysis of these binary CO_2 mixtures, please refer to Paper V and Report VIII.

Table 2.9 AAD of EOS on the calculated VLE properties of binary CO_2 mixtures

		PR	PT	RK	SRK	3P1T
CO_2/CH_4	P_s	2.91	2.32	5.25	2.66	21.52
	$y_{s,CO2}$	3.12	3.62	20.31	3.71	28.49
CO_2/O_2	P_s	5.12	4.54	6.30	4.97	9.65
	$y_{s,CO2}$	3.91	3.74	13.19	4.65	7.85
CO_2/H_2S	P_s	1.22	3.65	3.95	1.32	3.32
	$y_{s,CO2}$	4.54	10.82	11.91	4.49	4.79
CO_2/N_2	P_s	6.04	5.86	14.17	11.28	9.65
	$y_{s,CO2}$	3.80	3.76	9.95	6.08	7.85
CO_2/Ar	P_s	5.01	5.00	8.01	5.32	25.75
	$y_{s,CO2}$	-	-	-	-	-
CO_2/SO_2	P_s	4.76	4.79	10.62	4.33	12.02
	$y_{s,CO2}$	-	-	-	-	-

2.3.3.2 Prediction of Volume

For the calculation on volume, 3P1T was replaced by three other equations due to its poor performance on VLE.

- MSRK and MPR EOS include a translation along the volume axis. Applications of this improved method to pure liquid, mixtures of liquids or gases, and petroleum fluids show that markedly superior volume estimations are obtained, except in the neighbourhood of the pure-component critical points; nonetheless, critical volumes for mixtures can be estimated correctly [64].
- ISRK [65] EOS is another modification of SRK, by introducing a temperature dependent volume correction. ISRK can provide accurate volumes for polar and non-polar pure substances both near to and far from the critical point. It can also be easily extended to mixtures, and the calculation results show that it can shift the critical locus towards experimental values and give good results for the liquid volumes of mixtures.

Table 2.10 Supplement cubic EOS for volume calculations

EOS	Function Form	Mixing Rule
MPR	$P=\frac{RT}{V-b}-\frac{a}{(V+c)(V+b+2c)+(b+c)(V-b)}$	$a=\sum_i\sum_j x_i x_j a_i^{1/2} a_j^{1/2}(1-k_{ij})$; $b=\sum_i x_i b_i$; $c=\sum_i x_i c_i$; $k_{ij}=k_{ji}$
MSRK	$P=\frac{RT}{V-b}-\frac{a}{(V+c)(V+b+2c)}$	$a=\sum_i\sum_j x_i x_j a_i^{1/2} a_j^{1/2}(1-k_{ij})$; $b=\sum_i x_i b_i$; $c=\sum_i x_i c_i$; $k_{ij}=k_{ji}$
ISRK	$P=\frac{RT}{V+c-b}-\frac{a(T)}{(V+c)(V+b+c)}$	$a=\sum_i\sum_j x_i x_j a_i^{1/2} a_j^{1/2}(1-k_{ij})$; $b=\sum_i\sum_j x_i x_j\left(\frac{b_{ii}+b_{jj}}{2}\right)(1-l_{ij})$; $c=\sum_i x_i c_i$; $k_{ij}=k_{ji}$; $l_{ij}=l_{ji}$

It has been mentioned that the proper value of k_{ij} may be different for different properties. Therefore, the k_{ij} calibrated from VLE data may not result in a high accuracy on the volume calculation. Figure 2-4 shows the AAD of PR EOS on the saturated pressure, the saturated vapour fraction of CO_2 ($y_{s,CO2}$), the gas volume and liquid volume of CO_2/CH_4 at different values of binary interaction parameter k_{ij}. It demonstrates that in order to pursue high calculation accuracy on volume, k_{ij} should be calibrated separately for gas and liquid phases. Table 2.11 lists the calibrated k_{ij} for volume calculations on both vapour and liquid phases.

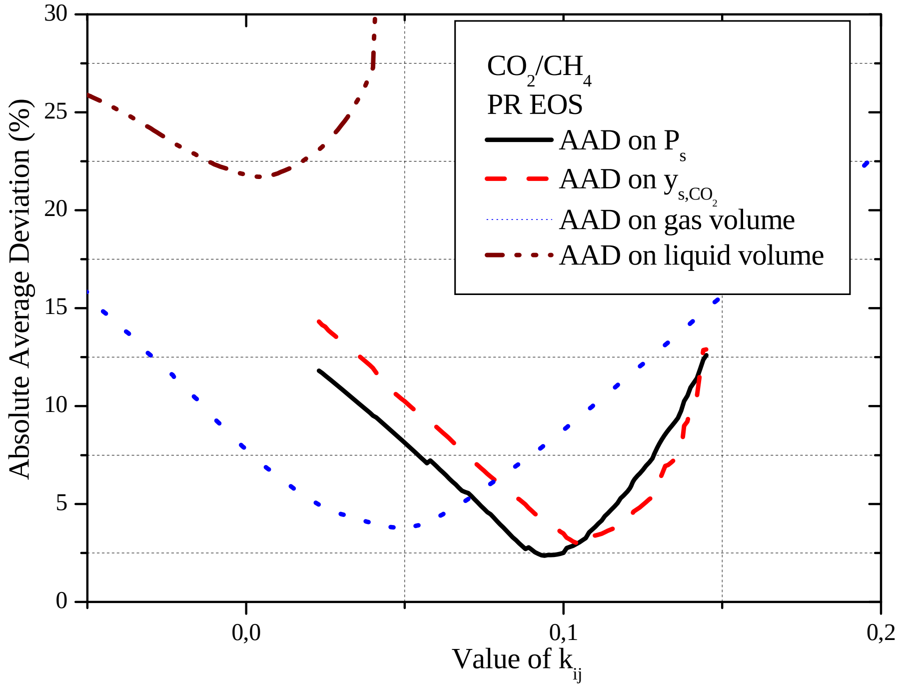

Figure 2.4 AAD of PR EOS on P_s, $y_{s,CO2}$, gas volume and liquid volume of CO_2/CH_4 at different k_{ij}

Table 2.11 Correlated k_{ij} for different binary CO_2 mixtures based on volume experimental data

		PR	PT	RK	SRK	MPR	MSRK	ISRK*
CO_2/CH_4	G	0.049	0.963	0.008	0.018	-0.006	-0.032	0.033/0.189
	L	0.008	1.002	-0.077	-0.056	-0.120	-0.192	-2.225/-0.375
CO_2/H_2S	G	0.038	0.960	0.031	0.033	-0.014	-0.015	-0.055/0.125
	L	0.012	1.004	-0.073	-0.064	-0.082	-0.181	-0.900/-0.085
CO_2/N_2	G	-0.001	1.015	-0.019	-0.037	-0.053	-0.095	-0.104/0.099
	L	-0.017	1.029	-0.129	-0.104	-0.154	-0.258	-0.490/0.050
CO_2/Ar	G	0.027	0.990	0.0	0.007	-0.031	-0.043	0.015/0.320
	L	0.002	1.015	-0.077	-0.065	-0.124	-0.200	-0.015/0.335
CO_2/SO_2	G	-0.085	1.090	-0.091	-0.092	-0.148	-0.156	-0.500/-0.500
	L	0.004	0.996	-0.026	-0.026	-0.122	-0.175	-0.700/-0.115

* k_{ij}/l_{ij}

Tables 2.12 shows the absolute average deviations of equations of state on the gas and liquid volumes of CO_2 mixtures respectively, which were calculated with different values of k_{ij}. It is same to the calculations on VLE properties that the performances of EOS vary for various mixtures. More concrete evaluations are available in Paper VIII.

Table 2.12 AAD of EOS on both gas and liquid volumes of binary CO_2 mixtures (%)

		PR	PT	RK	SRK	MPR	MSRK	ISRK
CO_2/CH_4	V_g	2.95	2.34	2.56	2.56	4.49	3.97	7.42
	V_l	4.17	3.70	5.19	5.12	5.50	6.08	8.33
CO_2/H_2S	V_g	4.71	5.57	8.84	7.34	3.37	4.26	7.21
	V_l	3.03	2.43	4.95	4.18	4.30	4.97	4.99
CO_2/N_2	V_g	1.58	0.98	1.47	1.50	2.85	2.59	5.17
	V_l	1.74	1.77	5.97	4.99	3.79	6.16	7.46
CO_2/Ar	V_g	5.96	6.08	6.43	6.45	7.21	7.16	6.24
	V_l	2.37	2.12	4.86	4.66	3.99	5.48	4.64
CO_2/SO_2	V_g	13.02	13.06	14.26	14.00	11.64	12.76	8.83
	V_l	9.43	9.28	11.96	10.84	10.51	12.15	13.21

2.4 Discussions

2.4.1 Experimental Data

Regarding the CO_2 mixture, the TPX ranges of experimental data do not completely match the operation conditions of the CCS processes. This will result in poor evaluation results of the theoretical models because no sufficient experimental data are available for verifying the models. For example, there are only 4 experimental results at the same temperature about VLE and liquid volume of CO_2/Ar. Based upon such experimental data, the verified model may not be able to provide accurate results, when temperatures are beyond this temperature. Moreover, the experimental data of CO_2/SO_2 mixtures are old. Updated experimental data are, therefore, needed to reduce the uncertainty of the evaluations.

2.4.2 Calculation Models

To all cubic EOS considered in this study, k_{ij} has significant effects on the calculating accuracy and the application range of an EOS. Those equations have better accuracy on VLE with calibrated k_{ij} than with the default value of k_{ij}. Therefore, if a new impurity is introduced in CO_2 mixtures, the calibrated k_{ij} of CO_2/new-impurity should be obtained in order to assure a high reliability. Moreover, as aforementioned, kij was calibrated as a constant in the calculations of CO_2 mixtures. To further improve calculation accuracy, there are two options to handle k_{ij}. One way is that k_{ij} could be calibrated to a function of temperature and pressure, perhaps even of composition, when sufficient experimental data are available. The other way is to calibrate k_{ij} in narrow T, P, x and y ranges, by which the calculation accuracies could be improved for most interested conditions. This, however, will seriously reduce the applicability in extended ranges.

2.4.3 Suggestions Regarding Method Selections

Calculating accuracies of different EOS on VLE and volume are evaluated. With recommended EOS, the most of AAD on parameters of VLE are within 5%, while AAD on volume are within 10% except those of CO_2/SO_2. Detailed results are summarized in Table 2.13.

Table 2.13 Recommended equations of state and their corresponding accuracies for predicting VLE and volume of different CO_2 mixtures

Mixtures	ACD on VLE (%)			ACD on Volume (%)			
	EOS	P_s	y_s	EOS	V_g	EOS	V_l
CO_2/O_2	PT	4.54	3.74	-	-	-	-
CO_2/N_2	PT	5.86	3.76	PT	0.98	PR	1.74
CO_2/SO_2	SRK	4.33	-	ISRK	8.83	PT	9.28
CO_2/Ar	PT	5.00	-	PR	5.96	PT	2.12
CO_2/H_2S	PR	1.22	4.54	MPR	3.37	PT	2.43
CO_2/CH_4	PR	2.91	3.12	PT	2.34	PT	3.70

2.4.4 Future Work

Based upon the above analysis, to improve the reliability of evaluation, future work is necessary in the areas of:

- Carrying out more accurate experiments, especially on VLE of CO_2/Ar, CO_2/SO_2, and CO_2/N_2, VLE at pressures higher than 8.5MPa, and on volume of CO_2/O_2, CO_2/SO_2 and CO_2/Ar;
- Including evaluations on the ternary CO_2 mixture to further verify the theoretical models for the calculations of multi-components systems;
- Calibrating the binary interaction parameter to a polynomial instead of a constant, or in a narrow application range to further improve the calculation accuracy on VLE of EOS.

3 Impact of Impurity on Thermodynamic Properties of CO_2 Mixtures and Different Processes Involved in the CCS Systems

By changing the thermodynamic properties of CO_2 mixtures, impurities have great impact on system design, operation, and optimization. For example, the relationships between thermodynamic properties and some system parameters of CO_2 purification and transportation are summarized in Table 3.1.

Table 3.1 Relationship between thermodynamic properties and system parameters

		Operation conditions		Energy consumption		Configuration Design		Performance	
		PUR	TRA	PUR	TRA	PUR	TRA	PUR	TRA
VLE	DP	√		√				√	
	BP		√	√			√	√	
	DBDP			√		√			
Heat Capacity				√	√				
Enthalpy and entropy				√	√				
Volume							√		√

The variation of impurity content will influence the VLE properties of CO_2 mixtures, which mainly mean the boiling and condensing behaviours. Physical separation shall be conducted in two-phase area, which implies that at a constant temperature, the operation pressure should be above the condensing pressure and below the boiling pressure of the mixtures. Different from separation, transportation must be carried out above their boiling pressure for safety issues. Therefore, when the VLE properties are changed, the operation conditions of the CO_2 compression/purification (e.g. the discharging pressure of compression and the condensation temperature) and transport systems should also be changed accordingly. Meanwhile, the CO_2 purity of the separation product is the CO_2 mole fraction of bubble point. Thus, when the boiling behaviour is changed, the performance of separation would be changed. In addition, the configuration of separation unit is tightly related to the difference between boiling and dew points. If there is a big difference between boiling and dew points, separation system can be simpler. For instance, multi-stage flash may be used instead of distillation column, which is required for separating mixtures with close boiling and dew points.

The variation of impurity content will also influence the enthalpy, entropy and heat capacity of CO_2 mixtures. Since the energy consumptions of compression and refrigeration are determined by the enthalpy and entropy changes in those processes, as a result, impurities can have impacts on the energy consumption.

Moreover the variation of impurity content will vary the effective CO_2 volumes (ECV) of CO_2 streams, which is defined as:

$$ECV = \frac{V_{CO_2}}{V_{CO_2-mixture}} \tag{3.1}$$

ECV can directly affect the efficiencies and economic issues of CO_2 transport and storage; therefore, it is significant to the design of CO_2 transport and storage systems.

Compared with other approaches for CO_2 capture, such as pre-combustion capture and post-combustion capture, relatively high levels of impurities are expected in the captured CO_2 streams from oxy-fuel combustion. So it presents more challenges for CO_2 processing processes, which includes dehydration, purification and compression [66]. Here efforts were mainly focused on the impurities appearing in the oxidizing CO_2 streams captured from oxy-coal combustion. In this chapter, the impact of impurities on the thermodynamic properties of CO_2 mixtures was firstly analyzed; then the impact of impurities was further discussed concerning different processes involved in the CCS systems.

3.1 Impact of Impurity on Thermodynamic Properties of CO_2 Mixtures

According to Table 3.1, the impact of impurity on VLE, Heat capacity, enthalpy and volume were investigated respectively, considering their importance to the system design and operation.

3.1.1 Impact on VLE

Figure 3.1 shows an example of the phase diagrams of CO_2/Ar, CO_2/N_2 and CO_2/O_2 at 223.15K. In the area marked A, the CO_2 mixtures are in the liquid phase; in the area marked as C, they are in the gas phase; in the area marked as B, which is between A and C, two phases co-exist. In order to better understand the VLE behaviours of CO_2 mixtures in the CCS applications, the concentration ranges of impurities were reduced to the probable concentrations of impurities that appear in the CCS processes. Referring to the composition windows of different components presented in the Section 2.1, the mole fractions of Ar, N_2 and O_2 were set between 0-5%, 0-15%, and 0-7% respectively, as shown in the right side diagrams in Figure 3.1.

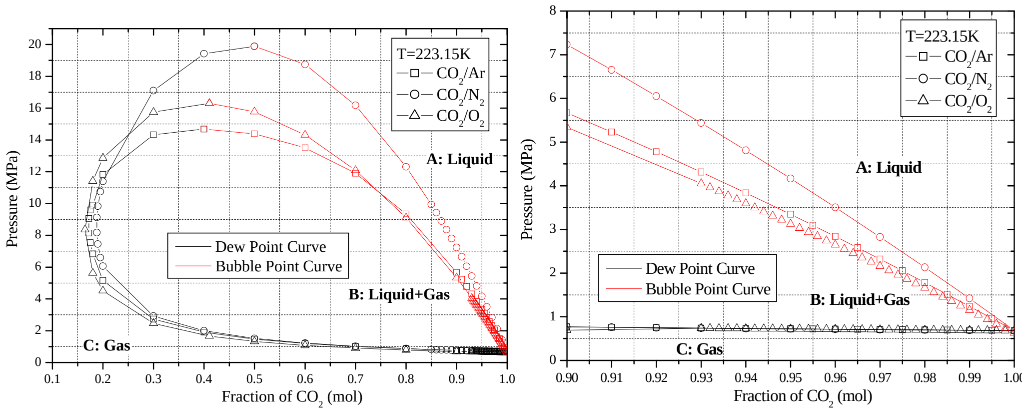

Figure 3.1 Comparison of VLE characteristics among the binary CO_2 mixtures containing non-condensable impurities: Ar, O_2 and N_2

Compared with the saturated state of pure CO_2, the increment of non-condensable gases makes both the boiling pressure and condensing pressure of CO_2 mixtures rise. For relatively high purity of CO_2, for example, CO_2 >70 mol %, the impurities have a more clear impact on bubble point than on dew point. Comparatively, the variation of N_2 has the most remarkable impacts on both the dew points and the bubble points of CO_2 mixtures. Moreover, CO_2/N_2 has the biggest difference between bubble and dew points. The VLE characteristics of various CO_2 mixtures are shown in more details in Paper IV.

Different from the impacts of the non-condensable gases, SO_2 has the opposite impact of on the VLE properties of CO_2 mixtures. Figure 3.2 shows the VLE characteristics of CO_2/SO_2. Since SO_2 has a higher critical point than CO_2, the presence of SO_2 in CO_2 mixtures will make the condensing temperature increase at a certain pressure or conversely, make the condensing pressure decrease at a certain temperature.

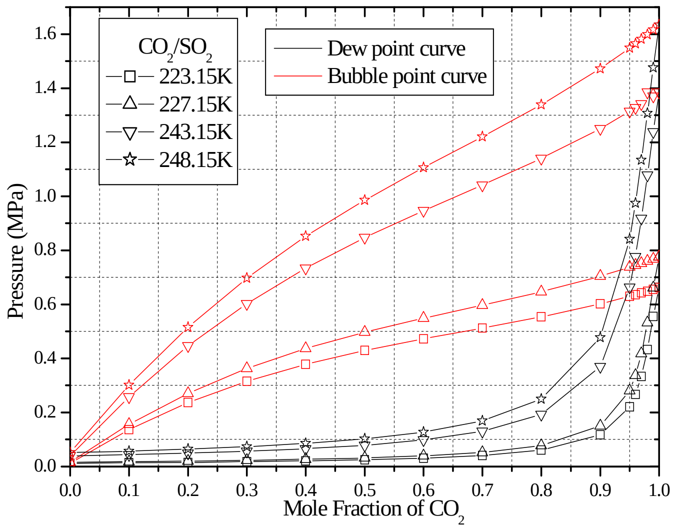

Figure 3.2 The VLE characteristics of the CO_2 mixtures containing condensable impurity SO_2

3.1.2 Impact on Heat Capacity

The heat capacity, enthalpy, and entropy are the important thermodynamic parameters of CO_2 mixtures, because they affect the heat transfer and energy consumption of the CO_2 compression/purification processes.

The temperature-dependent heat capacities of pure substance (C_{CO2}, C_{SO2}, C_{N2}, C_{O2} and C_{Ar}) have been calculated based upon an empirical equation [67]:

$$C = C_1 + C_2\left[\frac{C_3}{T}/\sinh(\frac{C_3}{T})\right]^2 + C_4\left[\frac{C_5}{T}/\cosh(\frac{C_5}{T})\right]^2 \tag{3.2}$$

and shown in Figure 3.3. The heat capacities of the pure substances decrease in an order of $C_{SO2} > C_{CO2} > C_{O2} > C_{N2} > C_{Ar}$. It is also clear that the heat capacities of O_2, N_2 and Ar are less temperature dependence.

The heat capacity of a CO_2 mixture could be calculated by following equation:

$$C_{mixture} = \sum_i^n C_i \times X_i \tag{3.3}$$

where C_i is the heat capacity of pure component. At the same operating temperature, the presence of SO_2 will increase, while the presence of Ar, O_2 and N_2 will decrease the heat capacities of CO_2 mixtures. This implies that the CO_2/SO_2 mixture may absorb or release more heat for the same changes in temperature at compared with that of CO_2/N_2, CO_2/O_2 and CO_2/Ar mixtures.

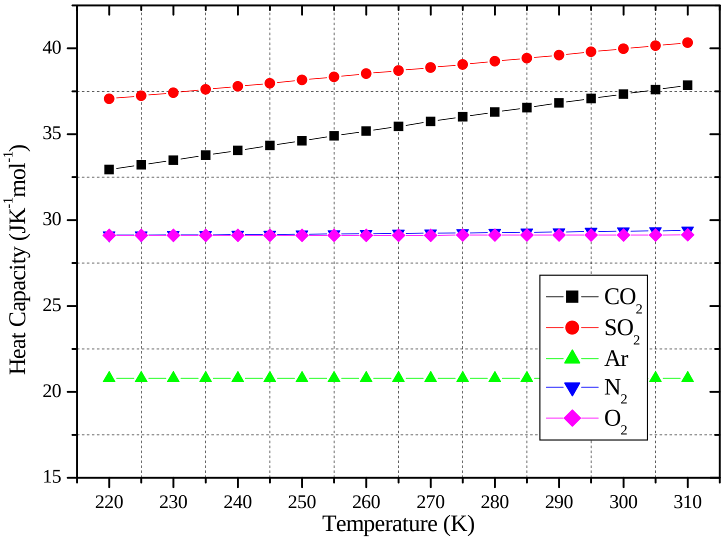

Figure 3.3 Heat capacity of different components at different temperatures

3.1.3 Impact on Enthalpy

The enthalpy of real gas can be calculated with the following equation:

$$h(t,p) = \int_{T_0}^{T} \sum y_i c_{p,i}{}^0 dT + \int_{p\to 0}^{p} \left[v - T\left(\frac{\partial v}{\partial T}\right)_p \right] dP \tag{3.4}$$

Figure 3.4 shows the enthalpies of different CO_2 mixtures at 303.15K and 3MPa. It is clear that only the presence of SO_2 increases the enthalpy of CO_2 mixtures, which is mainly due to its heat capacity being higher than that of CO_2. More discussion about the impacts of impurities on enthalpy and entropy will be given in the analysis on energy consumption later.

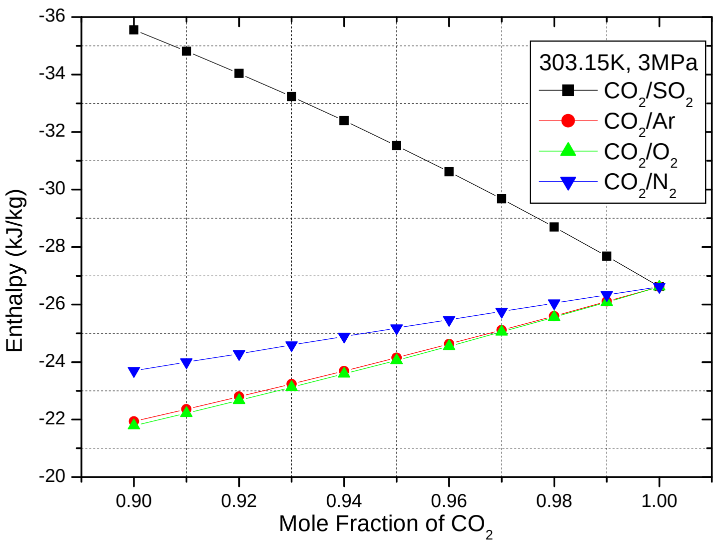

Figure 3.4 Enthalpy of different gaseous CO_2 mixtures

3.1.4 Impact on Volume

The impact of impurity on the volumes of CO_2 mixtures depends upon the molecular weights of impurities. Since the molecular weight of SO_2 is higher, while those of Ar, O_2 and N_2 are lower than that of CO_2, only SO_2 increases the molecular weight of CO_2 mixtures. As a result SO_2 makes the volumes of CO_2 mixtures increase while others make them decrease. Figure 3.5 shows the volumes and densities of binary CO_2 mixtures at different CO_2 compositions.

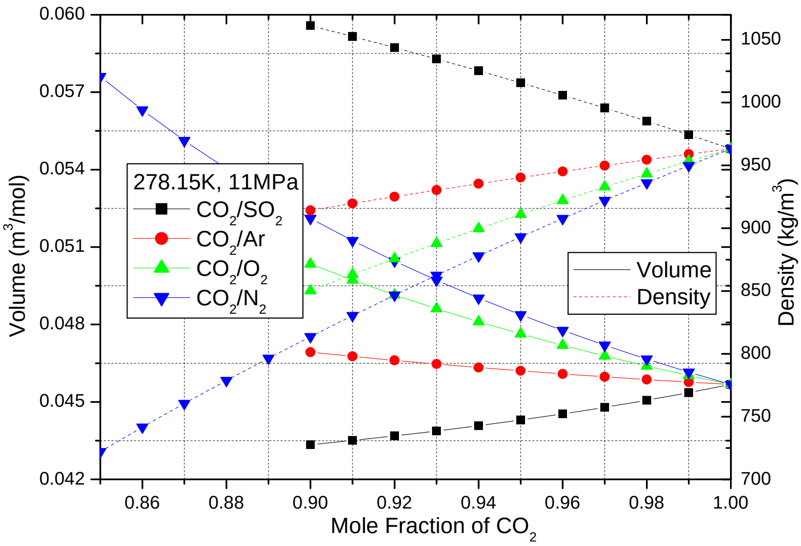

Figure 3.5 Volumes and densities of CO_2 mixtures at different CO_2 compositions

3.2 Impact of Impurity on the Different Processes Involved in the CCS Systems

3.2.1 Impact of Impurity on Purification

In order to satisfy the requirements of transportation and use the storage reservoir efficiently, non-condensable gases, such as O_2, N_2 and Ar should be removed from the CO_2 streams captured in the O_2/CO_2 recycle combustion. In this study, CO_2 purification process has been investigated with a focus on the physical separation of non-condensable gases. A simplified process flow diagram of purification is shown in Figure 3.6. The purification process includes three steps: CO_2 stream compression, CO_2 stream condensation/liquefaction, and non-condensable gas separation. After water removal, the CO_2 stream goes into the separation column, in which the CO_2 stream is condensed and non-condensable gases are separated. Then the CO_2 stream with higher purity will be transported to storage reservoirs by different measures.

The principle of physical separation is that the liquid/gas concentration of a component in a non-azeotropic mixture can be increased or decreased by varying the temperature or pressure of the mixture. Since those CO_2 mixtures containing O_2, N_2, and Ar are non-azeotropic, CO_2 streams can be purified by a physical separation, for example, using a distillation column or in a flash system.

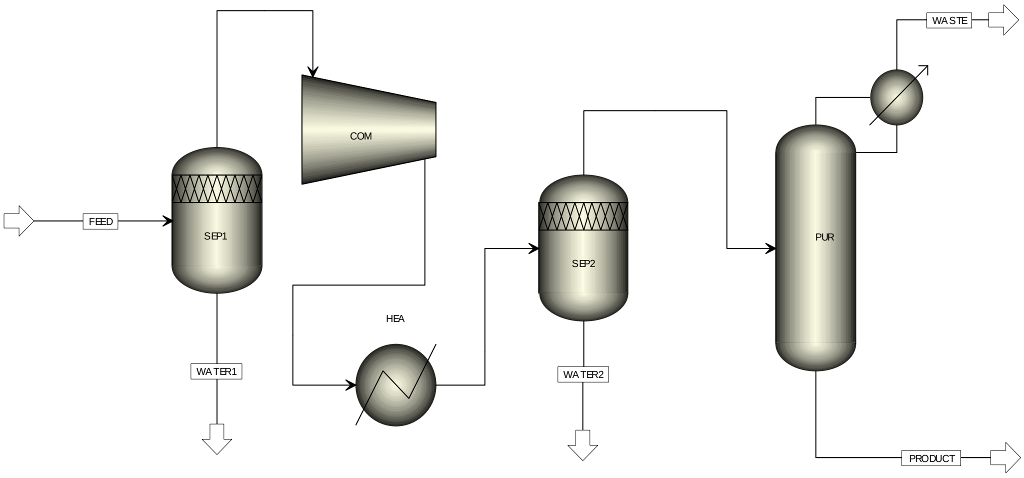

Figure 3.6 Simple process flow diagram of purification

The impact of impurity on non-condensable gas separation process is evaluated from the following aspects:

- Impacts on the operation conditions;
- Impacts on the purity of the liquid CO_2 product delivered to transport;
- Impacts on separation efficiency; and,
- Impacts on system configuration.

The operation conditions of purification are mainly determined by the dew points of CO_2 mixtures. Since the presence of non-condensable impurities increases the condensing pressures of CO_2 mixtures at a certain temperature, or decreases the condensing temperatures at a certain pressure, the increment of mole fractions of impurities increases either compression work or the energy demand of refrigeration. Comparatively, condensing CO_2 mixtures containing N_2 requires a lower condensing temperature or a higher condensing pressure than condensing mixtures containing other non-condensable gases. Therefore, the operation conditions of CO_2 purification can be more sensitive to the changes of N_2 concentration in CO_2 mixtures.

The purity of the liquid CO_2 obtained from the separation process is mainly determined by the bubble points of the CO_2 mixtures. From Figure 3.1, it can be found that the purity of liquid CO_2 mixtures decreases with the increase in pressure at a given temperature. It is also found that less N_2 exists in the liquid CO_2 product compared to that of Ar and O_2 at certain temperatures and pressures. This means that under the same operation conditions of purification, CO_2 purity of purification products is in an order of separating CO_2/N_2 > separating CO_2/Ar > separating CO_2/O_2.

How easily a non-condensable component can be separated from its corresponding CO_2 mixture can be evaluated by relative volatility [68] of the components, which is defined by:

$$\alpha_{AB} = \frac{y_{Ae} / x_{Ae}}{y_{Be} / x_{Be}} \tag{3.5}$$

where α_{AB} is the relative volatility of component *A* compared to component *B* when the two-component mixture under equilibrium conditions, y_{Ae}/y_{Be} and x_{Ae}/x_{Be} are the mole fractions of component *A*/*B* in vapour and liquid phase, respectively. As shown in Figure 3.7, N_2 has a higher relative volatility compared to Ar and O_2. This means that N_2 can be more easily separated from the CO_2 mixtures compared to the separation of Ar and O_2. It can also be found that pressure has more remarkable impacts on the relative volatilities of the non-condensable gases at low temperatures, such as 223,15K. These characteristics should be taken into account for the optimization of separation conditions.

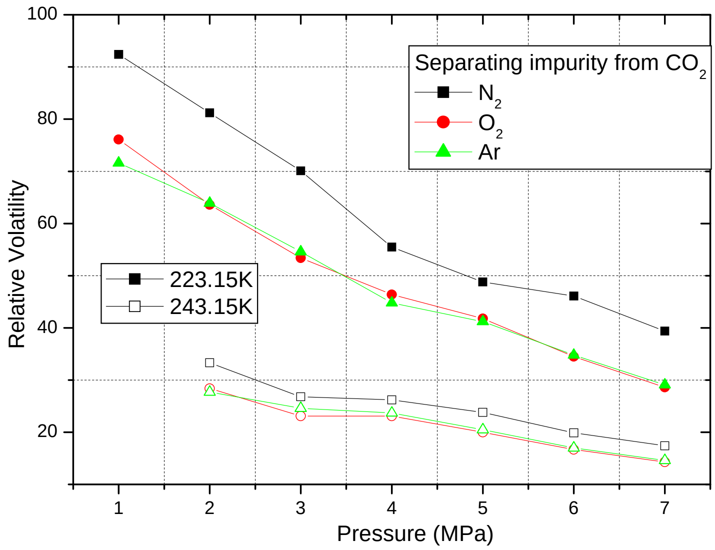

Figure 3.7 Relative volatilities of the non-condensable components involved in CO_2 mixtures

The system configuration of CO_2 purification is related to the difference between bubble and dew points of CO_2 mixtures. McCabe et al. [68] indicates:" flash distillation is used most for separating components which boil at widely different temperatures. It is not effective in separating components of comparable volatility since both the condensed vapour and residual liquid are far from pure". As the differences between bubble points and dew points of CO_2/N_2, CO_2/O_2 and CO_2/Ar are large; they can be purified by a flash system. Examples for simulating purification by flash and distillation tower are given in Paper IV.

3.2.2 Impact of Impurity on Compression

Compression can be conducted in a number of ways, such as undergoing an isothermal path, a polytropic path, or an isentropic path. If we ignore the change of kinetic energy and potential energy, theoretical compression work is reduced as the compression path approaches the isothermal from the isotropic.

In an actual compression process, the isothermal compression is unable to be realized and consequently it is a polytropic process. Due to the diversification of polytropic compression, the impact of impurity on isothermal compression and isentropic compression, which are the top and bottom limits of polytropic compression work, was studied instead.

Figure 3.8 shows the work required for compressing different CO_2 streams isothermally at different outlet pressures and different CO_2 compositions. Under the same operation conditions, compressing CO_2/SO_2 will consume the least work, while compressing CO_2/N_2 will require the most work. Meanwhile, compression work increases along with the increments of Ar, O_2 and N_2; while decreases along with the increment of SO_2 linearly, if the outlet pressure is constant.

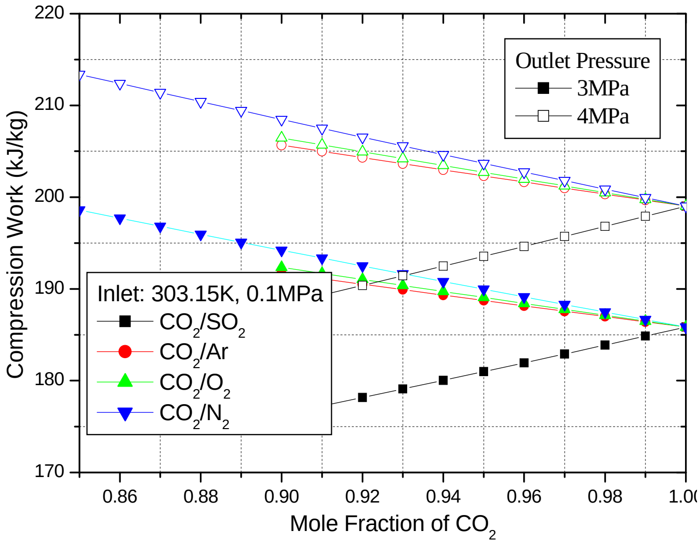

Figure 3.8 Energy consumption of isothermal compression at different CO_2 compositions

Figure 3.9 shows the discharging temperatures and energy consumption of isentropic compression. It can be seen that Ar, O_2, and N_2 make discharging temperature increase, while SO_2 makes it decrease. Comparatively, the discharging temperature is more sensitive to the fraction variation of Ar than other impurities. Meanwhile impurities affect the isentropic compression work in similar ways as they affect the discharging temperature.

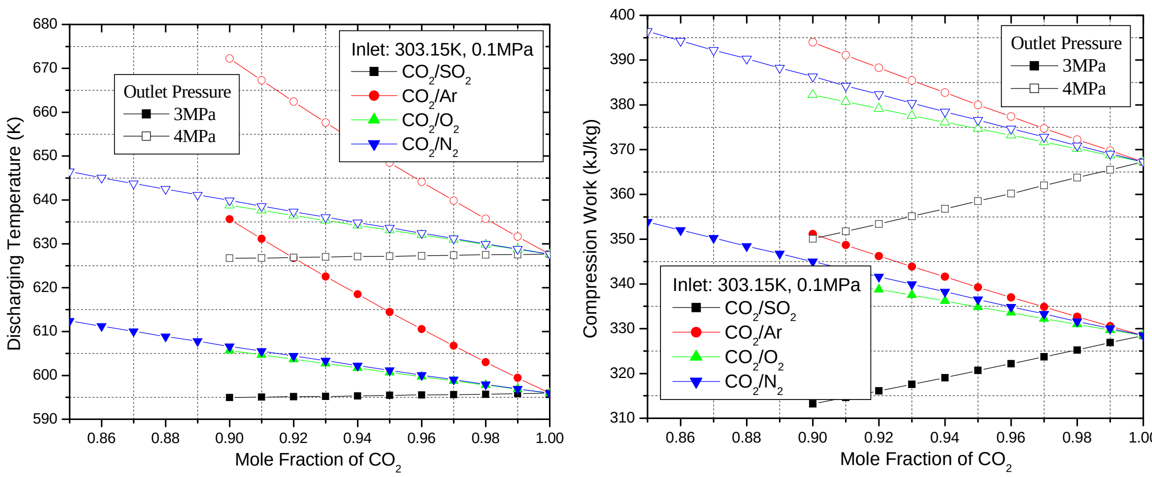

Figure 3.9 Discharging temperature and energy consumption of isentropic compression at different CO_2 compositions and pressures

Figure 3.10 compares the compression work between isothermal and isentropic processes. It is clear that the energy consumption difference becomes larger along with the rise of the concentrations of non-condensable gases. This implies that it is more desirable to compress the CO_2 mixture containing non-condensable gases in the process that is close to isothermal compression. In other words, intercooling shall be considered in the compression of CO_2/O_2, CO_2/N_2 and CO_2/Ar, especially at relatively high impurity concentrations.

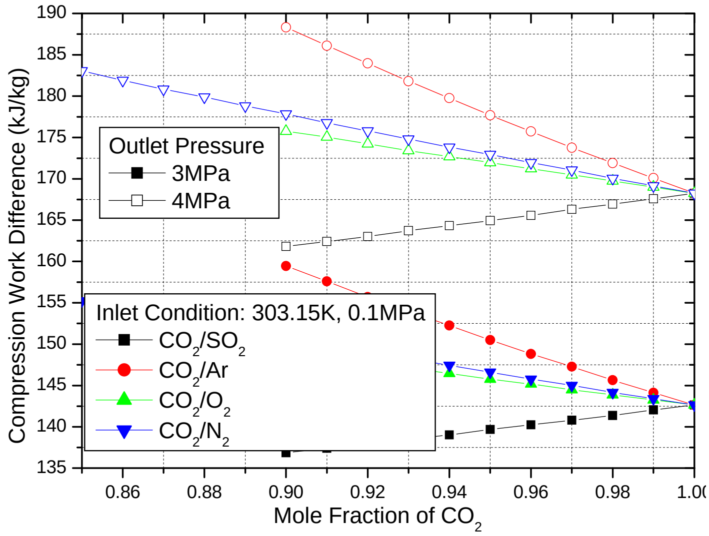

Figure 3.10 Comparison on the compression work of isothermal and isentropic processes

3.2.3 Impact of Impurity on Refrigeration/Liquefaction

In order to liquefy CO_2 mixtures, two ways can be applied to remove heat from the gas processing system: (1) cooling the gas by transferring heat to a cold reservoir (external refrigeration); and, (2) using Joule-Thomson effect, which is called *self-refrigeration*. In this study, the external refrigeration is investigated to understand the impacts of the impurities on the demands of refrigeration for the phase separation of the CO_2 mixtures.

Figure 3.11 shows the energy consumption of external refrigeration at different inlet and outlet temperatures and pressures. Refrigeration duty rises along with the drop of the discharging temperatures of refrigeration and operating pressures. Meanwhile, refrigeration decreases with the increments of non-condensable impurities; while increases with the increments of SO_2 due to the impact of impurity on heat capacity. In addition, there is a turning point on their curves of the required refrigeration for liquefying CO_2/Ar, CO_2/O_2 and CO_2/N_2. Before and after that point, the increasing rates of the energy demand with the decrements of impurity are different. The reason for this difference comes from the fact that CO_2 mixtures are partially condensed before the point, and the decrement of impurities will increase the liquid fraction. Due to the latent hear of phase change, the energy consumption of refrigeration increases faster when more fractions are liquefied.

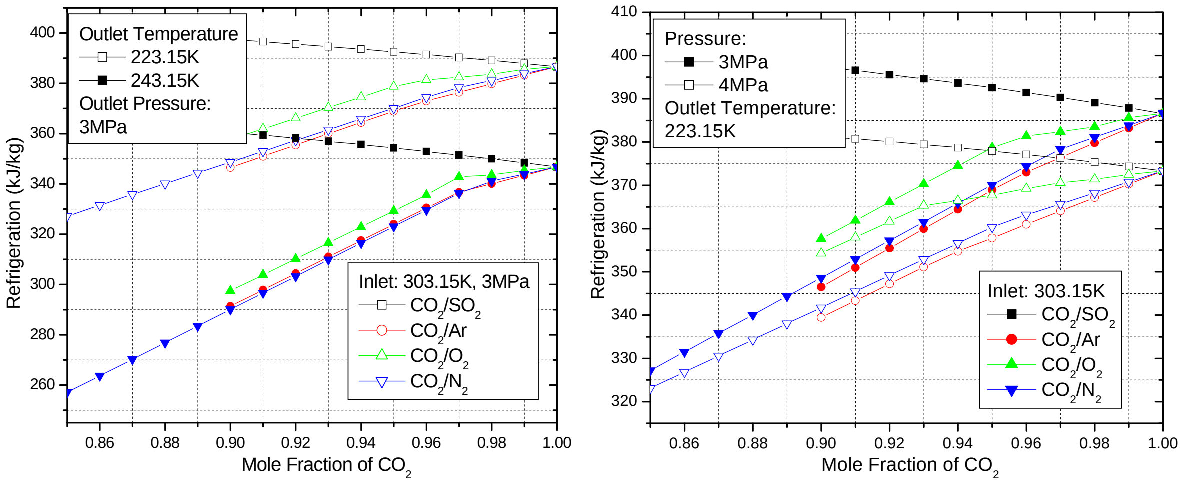

Figure 3.11 Energy consumption of external refrigeration required by CO_2 liquefaction at different CO_2 compositions and operation conditions

3.2.4 Impact of Impurity on CO_2 Transportation

To improve transportation efficiency, it is preferable to transport CO_2 in a high-density state. The desired state of the CO_2 fluids is different based upon the means of transportation. For transportation in vessels, liquid phase in low pressure is desirable [13]. If CO_2 is transported in pipeline, liquid phase in high pressure, or supercritical phase is desirable. However, regardless of which transport method is used, phase change must be avoided to ensure the safety of transportation.

3.2.4.1 Acceptable Concentration Ranges of Non-condensable Impurities

To guarantee the safe transportation of CO_2 mixtures, the concentrations of non-condensable impurities should be restricted in appropriate ranges. According to the estimated T-P windows for CO_2 transport (Table 2.2) and possible concentration ranges of the impurities, the potential of phase changes under such conditions is presented. Results on the acceptable maximum mole fraction of impurities at the given temperature and pressure are summarized in Table 3.2.

As shown in Table 3.2, very low contents of the non-condensable impurities should be kept for the CO_2 products for the vessel transport. Especially, the operation conditions of the transport in large tanks should be carefully investigated again, because the VLE calculations show that the CO_2 mixtures may be in a gas phase even when the purity of CO_2 is 100%. For example, at 218.15K, 5bar cannot satisfy the requirement transporting CO_2 mixtures in liquid phase.

Table 3.2 Acceptable maximum mole fraction of impurities at the given temperatures and pressures

Pressure (MPa)	Temperature (K)									
	Large tank			**Small tank**			**Pipeline**			
	218.15	223.15	228.15	238.15	243.15	248.15	273.15	283.15	293.15	303.15
Acceptable N_2 content in CO_2/N_2 mixtures (mol%)										
0.5	Gas[1]	Gas[1]	Gas[1]	-	-	-	-	-	-	-
0.7	0.18	0.03	Gas[1]	-	-	-	-	-	-	-
0.9	0.45	0.30	0.10	-	-	-	-	-	-	-
1.0	-	-	-	Gas[1]	Gas[1]	Gas[1]	-	-	-	-
1.5	-	-	-	0.57	0.14	Gas[1]	-	-	-	-
2.0	-	-	-	1.52	1.12	0.63	-	-	-	-
2.5	-	-	-	2.30	2.10	1.62				
8.0	-	-	-	-	-	-	9.54	7.88	5.70	4.33
>9.0	-	-	-	-	-	-	15[2]	15[2, 3]	15[2, 3]	15[2, 3]
Acceptable Ar content in CO_2/Ar mixtures (mol%)										
0.5	Gas[1]	Gas[1]	Gas[1]	-	-	-	-	-	-	-
0.7	0.24	0.03	Gas[1]	-	-	-	-	-	-	-
0.9	0.60	0.40	0.12	-	-	-	-	-	-	-
1.0	-	-	-	Gas[1]	Gas[1]	Gas[1]	-	-	-	-
1.5	-	-	-	0.45	0.11	Gas[1]	-	-	-	-
2.0	-	-	-	1.20	0.88	0.50	-	-	-	-
2.5	-	-	-	1.97	1.67	1.29	-	-	-	-
8.0	-	-	-	-	-	-	5[2, 3]	5[2, 3]	5[2, 3]	4.60
>9.0	-	-	-	-	-	-	5[2, 3]	5[2, 3]	5[2, 3]	5[2, 3]
Acceptable O_2 content in CO_2/O_2 mixtures (mol%)										
0.5	0.05	Gas[1]	Gas[1]	-	-	-	-	-	-	-
0.7	0.43	0.14	Gas[1]	-	-	-	-	-	-	-
0.9	0.83	0.52	0.25	-	-	-	-	-	-	-
1.0	-	-	-	Gas[1]	Gas[1]	Gas[1]	-	-	-	-
1.5	-	-	-	0.65	0.21	Gas[1]	-	-	-	-
2.0	-	-	-	1.59	1.14	0.64	-	-	-	-
2.5	-	-	-	2.55	2.09	1.59	-	-	-	-
8.0	-	-	-	-	-	-	7[2, 3]	7[2, 3]	6.04	4.68
>9.0	-	-	-	-	-	-	7[2, 3]	7[2, 3]	7[2, 3]	7[2, 3]

Notes: [1] in gas phase even for pure CO_2; [2] the max tested impurities content in corresponding CO_2 mixtures; [3] in supercritical liquid phase or supercritical fluid phase.

3.2.4.2 Transport Efficiency

In most cases, CO_2 is transported and stored in a supercritical state. The volume of CO_2 mixtures significantly affects the efficiency and safety of CO_2 transportation and storage. For example, the higher the effective CO_2 volume is, the more efficiently the CO_2 can be transported, and the more efficiently the pore space in geological media can be used for storage. In addition, the buoyancy forces decrease with the increase of CO_2 mixture density. It would be easier to reduce CO_2 leakage from the top rock layer of storage sites if the buoyancy force is lower.

Figure 3.12 shows the effective CO_2 volumes, calculated based on Equ. 3.1 under different mole concentrations and mass concentrations of CO_2. It is clear that occupied volumes by the given amount of impurities in corresponding CO_2 mixtures are in the following order: V_{N2} > V_{O2} > V_{Ar} > V_{SO2}. This means that N_2 has the worst impact on CO_2 transport efficiency and storage capacity, amongst all of impurities. Therefore its concentration should be kept as low as possible.

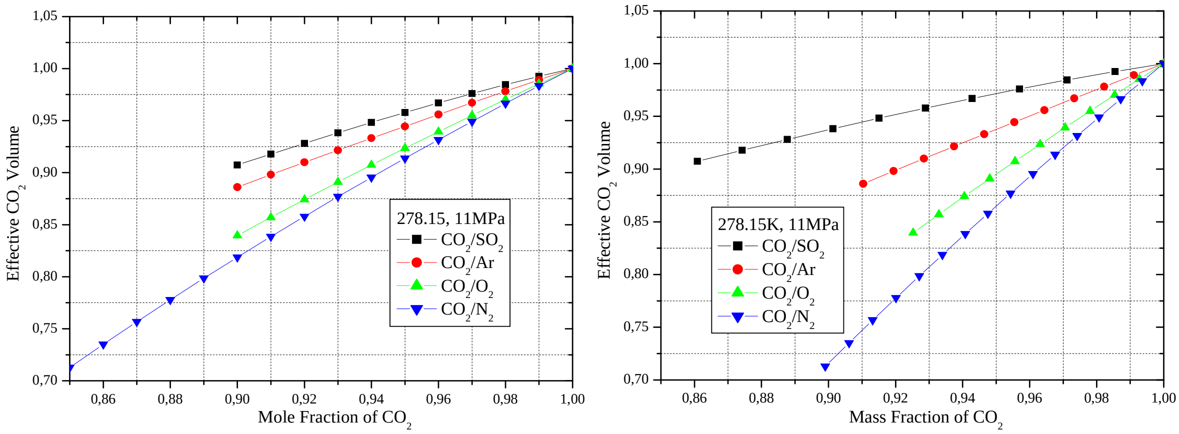

Figure 3.12 Effective CO_2 volumes of different CO_2 mixtures at different CO_2 mole and mass concentrations

3.3 Discussions

3.3.1 Impact of Impurity on the Thermodynamic Properties

In this chapter, the impacts of the impurities appearing in the oxidizing CO_2 stream (e.g. captured from oxy-fuel combustion) were mainly studied. However, it is different from the impurities appearing in the reducing CO_2 stream (e.g. captured from IGCC) that H_2S is found instead of SO_2. Moreover, H_2 is also important in the reducing CO_2 stream. Therefore, for the study on reducing CO_2 steams, the impacts of H_2S and H_2 should be investigated as well.

Current studies focus on the binary CO_2 mixture. However, the real flue gases are multi-component CO_2 mixtures. When there is more than one impurity, the changes of the properties of CO_2 mixtures and performances of different processes still remain unclear. Several questions must be answered before the evaluation results from the binary systems could be applied to the multi-component systems. For example, would the impact of impurity on thermodynamic properties be consistent in binary mixtures and multi-component mixtures? If there are several impurities, can the total impacts of impurities be decided simply by summing up the impact of any impurity? Which calculation methodologies are more suitable for the assessment of thermodynamic properties of the multi-component CO_2 mixtures?

In addition, hydrate formation and corrosion are tightly related to the content of water involved in CO_2 mixtures. H_2O is an important component for corrosion evaluation, especially for the CO_2 processing equipments located before the dehydration. However, the existence of other impurities, such as O_2, N_2, and Ar may change the solubility of water vapour. Therefore, it is essential to study the solubility of H_2O in multi-component CO_2 mixtures.

3.3.2 Compression

The results on the theoretical compression work of isothermal compression and isentropic compression have given some insights into the compression work of a multi-stage polytropic compression. However, the required compression power of an actual compression process is far from the theoretical compression work and is affected by many factors in addition to the impacts of impurities on the thermodynamic properties of CO_2 mixtures. For example, the impact of impurity on the transport properties of CO_2 mixtures, such as viscosity and heat conductivity, is also of great importance for the evaluation of the compression processes.

3.3.3 Refrigeration

As mentioned in Chapter 3.2.3, there are two ways to liquefy CO_2 streams. Comparatively liquefaction by external refrigeration is usually adopted when the process does not require very low temperatures [14]. Therefore, using Joule-Thomson effect to liquefy CO_2 streams might be more appropriated according to the desired operation conditions. In this research, the impact of impurity on the energy demand of refrigeration has been discussed based upon external refrigeration. However, impurities would have an impact on the energy consumption of self-refrigeration as well; because various impurities have different kinds of impacts on the latent heat of CO_2 mixtures and evaporating conditions. Therefore, further study should be conducted regarding the impact of impurity on self-refrigeration. In addition, the energy demand of refrigeration strongly depends upon the operation pressure. Hence, how to balance the energy consumption of compression and refrigeration is essential to the system optimization for CO_2 compression and purification.

3.3.4 Future Work

Based upon the current discussion, more work should be conducted to supplement the analysis of the impact of impurity on the thermodynamic properties of CO_2 mixtures. This includes:

- Investigating the impacts of H_2S and H_2 on the thermodynamic properties and the CCS processes; and,
- Investigating the impact of impurity in multi-component CO_2 mixtures and offering some general indications on the trends of this impact. Since very few experimental data about $CO_2/O_2/N_2$ exist, they will be used to verify the conclusions.

Part II: Evaporative Gas Turbine Cycles Integrated with CO_2 Capture

4 Evaporative Gas Turbine Cycles Integrated with Different CO_2 Capture Technologies

Performance of integrating CO_2 capture into a gas turbine cycle is significant in developing the innovative and optimal methods for CO_2 mitigation. A variety of system configurations to reach high efficiency and low CO_2 capture cost have been studied. For example, performance analysis has been conducted regarding the combined cycles (CC) integrated with different CO_2 capture technologies [69-72]. However, few studies are available concerning the integration of CO_2 capture with another advanced power cycle, the humidified gas turbine cycles.

Normally, humidified gas turbines include steam injection gas turbines (STIG) and evaporative gas turbines, also known as humid air turbine (HAT). The driving forces for gas turbine humidification have been the potentials of high electrical efficiency, specific power output, reduced specific investment cost, decreased formation of nitrogen oxides (NO_x) in the combustor, and, improved part-load performance compared with combined cycles [73]. In addition, compared with STIG, EvGT has a lower irreversibility, because water is injected into the cycle by humidification tower, which has a small temperature difference between the hot and cold fluids. This study is intended to analyze the integration of CO_2 capture with EvGT cycles.

Two CO_2 capture technologies are considered here including chemical absorption with MEA and O_2/CO_2 recycle combustion. The MEA-based chemical absorption technology is suitable for dilute systems and low CO_2 concentrations, and can be easily applied to the existing power plants. Thus far, this is the only commercially available option for CO_2 capture [74-78]. In the O_2/CO_2 recycle combustion option, the most promising features are the nearly 100% CO_2 capture and the simple CO_2 stream processing procedure, which does not involve absorption and stripping steps. However, on the other hand, it requires an air separation unit (ASU) to supply oxygen for combustion [79-81].

In this chapter, the performances of different configurations have been analyzed and compared from both technical and economical perspectives, in order to characterize and understand the features of the integration of EvGT with CO_2 capture process.

4.1 System Configurations

Two systems, as well as a reference system, are simulated with natural gas as fuel input. These include:

- System I (reference case): EvGT cycle without CO_2 capture;
- System II: EvGT cycle + chemical absorption capture; and,
- System III: EvGT cycle + O_2/CO_2 recycle combustion.

In order to avoid corrosion and the formation of ice or hydrate in CO_2 compression and transportation, the captured CO_2 streams will go through a dehydration process, after which the water content would be lower than 0.05% [82]. Furthermore, to achieve high cycle efficiency, waste heat is recovered for district heating from flue gas and the discharging streams of CO_2 compressors, stripper, and dehydrator through condensers or heat exchangers.

4.1.1 EvGT Cycle without CO_2 Capture

The basic idea of EvGT cycle is injecting water by evaporation, which will increase the mass flow rate through the turbine and, consequently, augment the specific power output. The EvGT cycle has a high efficiency, due to that fact the waste heat in the exhaust gas is recovered by humid air in the recuperator and by water in the economizer. A system sketch of EvGT cycle without CO_2 capture is shown in Figure 4.1. Water is heated close to saturation by the compressed air in the aftercooler, and flue gas in the feedwater heater and economizer. The heated water enters at the top of a humidification tower and is brought into counter-current contact with the compressed air that enters as the bottom of the tower. The tower is a column with a packing that is either structured or dumped. Some of the water is evaporated and the air is humidified. The water evaporates at the water boiling point corresponding to the partial pressure of water in the mixture, (i.e., water evaporates below the boiling point that corresponds to the total pressure in the tower). Therefore, low temperature heat, which cannot be used to evaporate water in a boiler, can be recovered in an EvGT cycle. Since the water vapour content in the air increases as the air passes upward through the tower, the boiling temperature also increases. This ensures a close matching of the air and water temperature profiles and small exergy losses, compared to the evaporation in a conventional steam boiler.

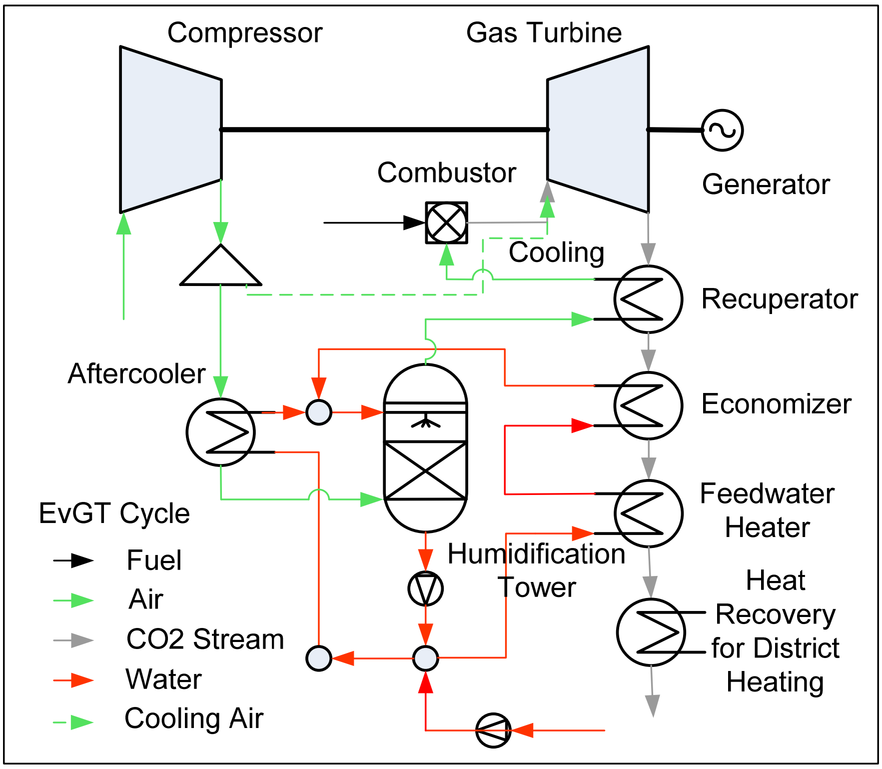

Figure 4.1 System sketch of System I (reference system): EvGT cycle without CO_2 capture

4.1.2 EvGT Cycle with Chemical Absorption CO_2 Capture

A system sketch of EvGT cycle with chemical absorption capture is shown in Figure 4.2. As opposed to System I, instead of being condensed in the feedwater heater, the flue gas enters the reboiler of MEA stripper to support the heat required for MEA regeneration; afterward, it goes through the recuperator and economizer. Then it is condensed in a heat exchanger, in which heat is recovered for district heating as well. After heat recovery, flue gas flows through the absorber counter-currently with the absorbent where the absorbent reacts chemically with CO_2. The rich solvent containing chemically bound CO_2 is then sent to the top of the stripper via a lean/rich cross heat exchanger, being heated to a temperature close to that of the stripper operating temperature. At an elevated temperature, the chemically bound CO_2 is released and absorber is regenerated in the stripper. After compression and dehydration, the recovered CO_2 will be transported to the storage reservoir through different means.

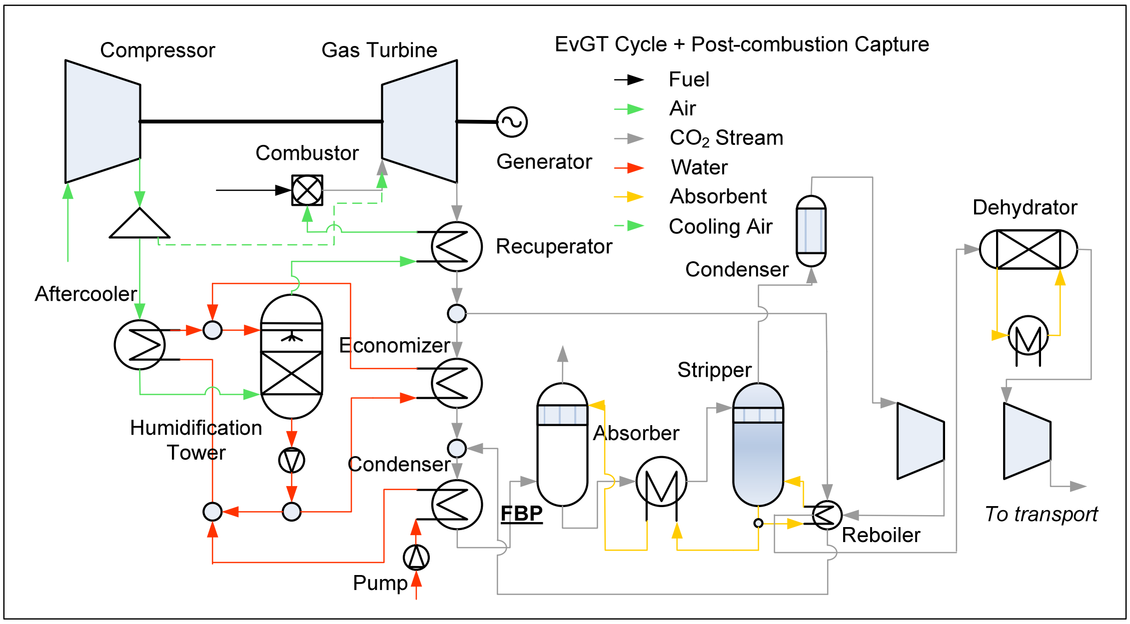

Figure 4.2 System sketch of System II: EvGT cycle with chemical absorption CO_2 capture

4.1.3 EvGT Cycle with O_2/CO_2 Recycle Combustion CO_2 Capture

A system sketch of EvGT cycle with O_2/CO_2 recycle combustion capture (oxy-fuel combustion) is shown in Figure 4.3. O_2/CO_2 recycle combustion takes place in a denitrogenation environment; it produces a flue gas that consists of mainly H_2O and CO_2. Therefore, a simplified flue gas processing procedure can be used instead of conventional means, such as chemical absorption, to achieve a low cost for CO_2 capture. For instance, flue gas could be compressed directly and transported to the storages after condensation and dehydration, without further purification. However, in the denitrogenation combustion, the nitrogen removal may cause the flame temperature to be extremely high and decrease the mass flow rate through the gas turbine. In order to compensate for the reduced mass flow, after condensation, a large fraction of flue gas is recycled back into the combustor. In addition, compared with the CO_2 capture approach of chemical absorption, relatively high levels of impurities are expected in the captured CO_2 streams from O_2/CO_2 recycle combustion. Here, the major impurity is oxygen, due to the existing amount of excess oxygen.

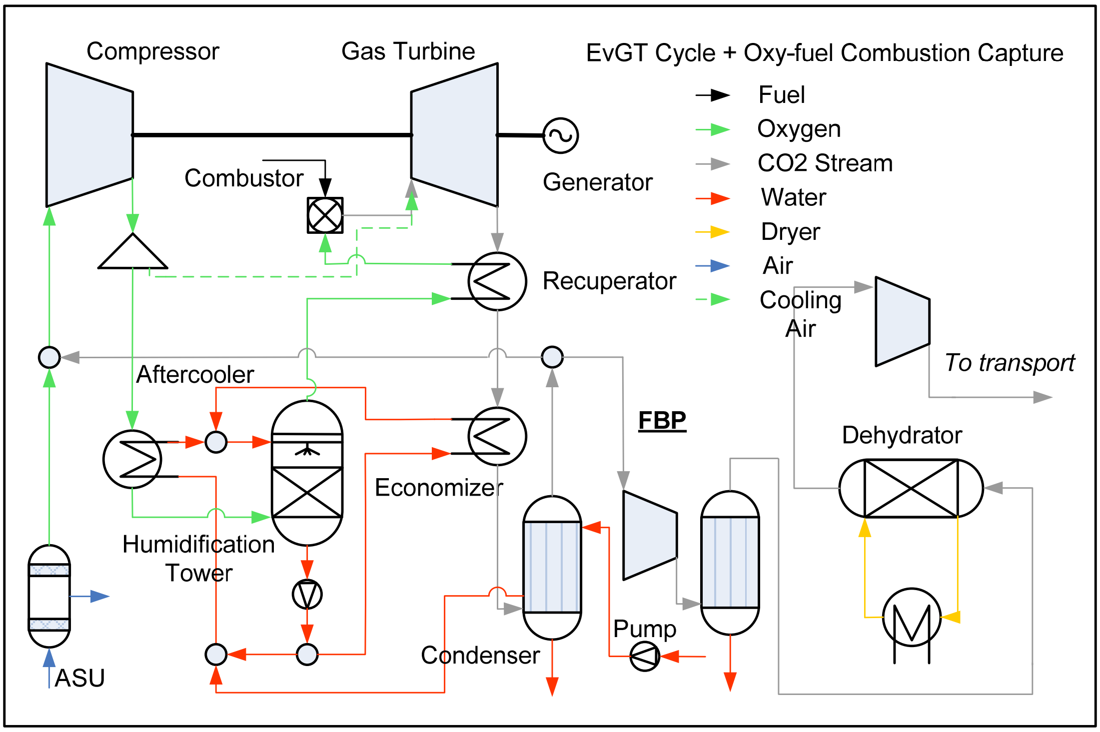

Figure 4.3 System sketch of System III: EvGT cycle with O_2/CO_2 recycle combustion CO_2 capture

4.2 Thermodynamic Performances of Various Systems

Systems have been simulated in Aspen Plus 2006. For chemical absorption capture process, the RADFRAC model is used for absorber and stripper columns. Meanwhile, the thermodynamic and transport properties were modelled using "*MEA property insert*", which describes the MEA-H_2O-CO_2 system with electrolyte-NRTL model [83]. In addition, PR equation of state is used for the calculations of thermodynamic properties in combustion, compression and other processes based upon our previous studies.

4.2.1 Input Data and Assumptions

Input data and assumptions for the simulations of gas turbine, compressors, chemical absorption, and dehydration are given in Table 4.1. Compositions and properties of inlet streams and outlet streams are summarized in Table 4.2.

Table 4.1 Input data and assumptions for the simulations of gas turbine, compressors, chemical absorption and dehydration

Parameter	Unit	Value
Turbine		
Pressure Ratio		20
Turbine Inlet Temperature (TIT)	K	1523.15
Mechanical Efficiency	%	99
Compressors		
Type		Isentropic
Isentropic Efficiency	%	85
Intercooling T	K	303.15
Stage Number of Air/Oxygen Compression		2
Stage Number of CO_2 Compression		3
Mechanical Efficiency	%	98
Chemical Absorption		
Solvent		MEA (30wt%)
Solvent Loading	$\frac{\text{Mol } CO_2}{\text{Mol MEA}}$	0.3
Stripper Operating P	MPa	0.1
Pressure Drop in Absorption Column	mbar	150 [72]
Dehydration		
Dryer		Triethylene glycol (TEG) (99 wt%)
Operating P of Dehydration	MPa	2.0
Operating P of Regeneration	MPa	0.1
Operating T of Regeneration	K	477.15 [84]
Others assumptions		
Pump mechanical Efficiency	%	90
Pressure Drop in Humidification Tower	%	5 [85]
ΔT_{min} Gas/Gas	K	30
ΔT_{min} Gas/Liquid	K	20
Supplying T for District Heating	K	60
CO_2 Capture Ratio of Chemical Absorption	%	90
Excess Oxygen in Flue Gas	mol%	3 [69]

In Table 4.1, the CO_2 capture ratio (CCR) has been defined as:

$$CCR = \frac{(\text{Mole flow} \times CO_2 \text{Mole fraction})_{CO_2 \text{ To be transported}}}{(\text{Mole flow} \times CO_2 \text{Mole fraction})_{\text{Flue gas to be processed}}} \tag{4.1}$$

Here, the flue gas to be processed is indicated as FBP in the Figure 4.2 and 4.3.

Table 4.2 Compositions and properties of feed streams and outlet streams

Fuel stream		
CH_4	%	100
LHV	MJ/kg	50
T	K	288.15
P	MPa	0.1
Air stream		
T	K	288.15
P	MPa	0.1
Composition		
N_2	vol%	76.99
O_2	vol%	20.65
Ar	vol%	0.921
CO_2	vol%	0.04
Relative Humidity	%	60
Oxygen stream		
T	K	288.15
P	MPa	0.1
Composition		
N_2	vol%	1
O_2	vol%	99
Energy Consumption	MJ/kg O_2	0.9 [70]
CO_2 Streams to be Transported		
T	K	293.15
P	MPa	15

4.2.2 Simulation Results and Discussions

With the same turbine inlet temperature and pressure ratio, three systems were simulated. Concrete evaluation results of EvGT integrated with CO_2 capture are given in Paper VI. Here, the system performance was analyzed from three perspectives: electrical efficiency, heat recovered for district heating, and CO_2 emission.

4.2.2.1 Electrical Efficiency

Figure 4.4 shows the breakdown of electricity generations and power consumptions in percentage of fuel energy (LHV-based) for the three systems. As can be seen from Figure 4.4, System I has the highest electrical efficiency, which is defined as:

$$\eta = \frac{\text{Net Electricity Generation}}{\text{Chemical Energy in Feul}} \tag{4.2}$$

with a value of 51.64%. The electrical efficiencies of System II and III are 39.73% and 37.45% respectively. Therefore, compared to System I, the penalty caused by CO_2 capture on electrical efficiency is 11.91 percentage point for System II and 14.19 percentage point for System III.

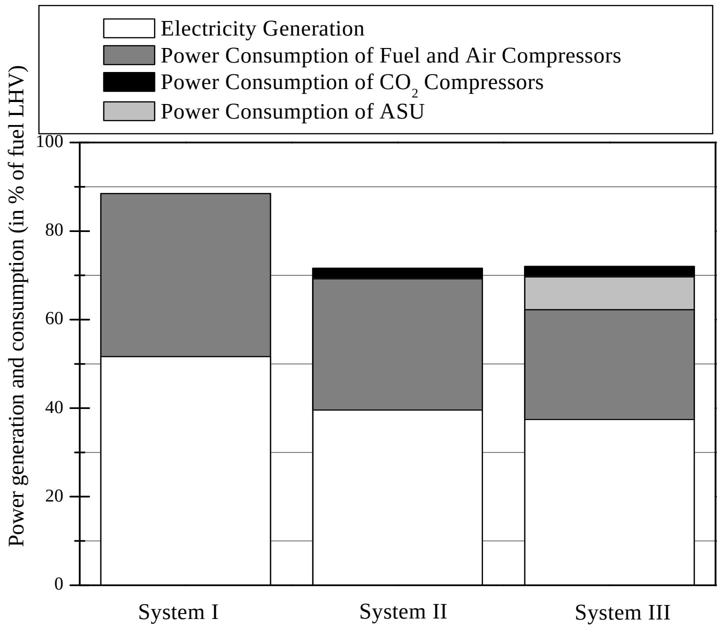

Figure 4.4 Breakdown of electricity generation and power consumption (in % of fuel LHV)

4.2.2.2 Heat Recovery

Figure 4.5 shows the breakdown of the heat consumption and the heat recovered for district heating in percentage of fuel input (LHV-based) for three systems. System III has the largest amount of heat recovered for district heating, which is about 28.9 in percentage of fuel LHV. Due to the heat recovered from the discharging flows of CO_2 compressors, more heat is recovered in System II and III than in System I. Meanwhile, because there is no heat demand by stripper, System III has more recovered heat than System II.

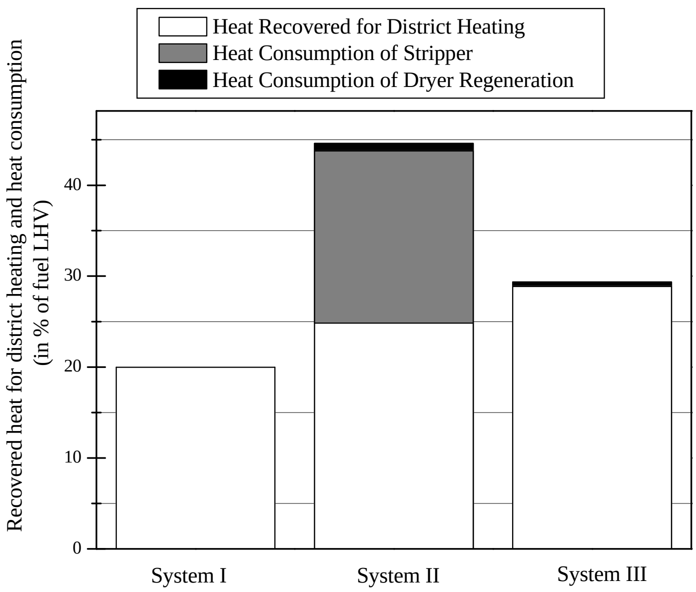

Figure 4.5 Breakdown of the heat recovered for district heating and heat consumption (in % of fuel LHV)

4.2.2.3 CO_2 Emission

The CO_2 emission per kWh produced electricity and the actual CO_2 capture ratio, which is defined as:

$$ACCR = \frac{(\text{Mole flow} \times \text{CO}_2 \text{ Mole fraction})_{CO_2 \text{ To be transported}}}{\text{Produced CO}_2\big|_{In \text{ combustion}}} \tag{4.3}$$

are presented in Figure 4.6. Compared to the CO_2 release of the EvGT cycle without CO_2 capture, 386g/kWh, the avoided CO_2 emissions of System II and III are 335g/kWh and 385g/kWh, respectively. The theoretical CO_2 capture ratios of System II and System III are 90% and 100%. However, in the real application, there will be slightly lower than the theoretical values because CO_2 may dissolve in the condensed water in condensers and be lost. Compared with System III, more water is condensed in System II. As a result, System II has a bigger reduction of CCR, 0.7 percentage point.

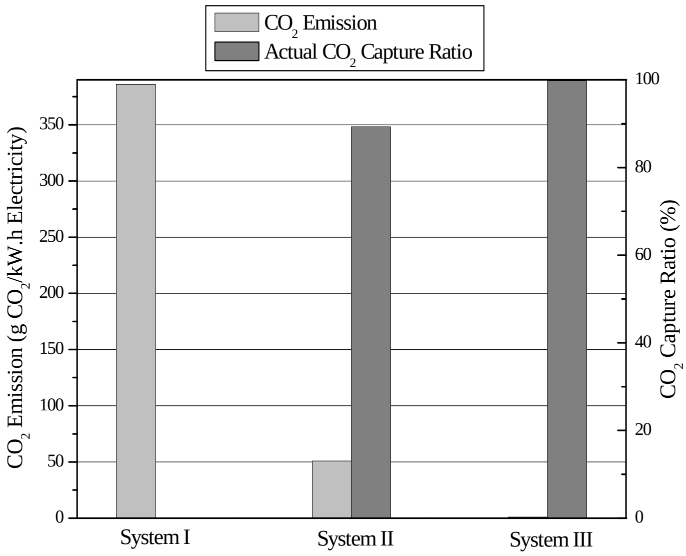

Figure 4.6 CO_2 emissions per kWh produced electricity and the CO_2 capture ratio

4.2.3 Compared with Combined Cycles

Kvamsdal et al. [72] investigated the performance of combined cycles (CC) with various CO_2 capture technologies. In Table 4.3, a comparison of electricity generation and internal electricity consumption is shown between CC and EvGT cycle. The CC always has a higher gross electricity generation, electricity efficiency, and internal electricity consumptions of Air/Fuel compressors. However, it has similar electricity consumptions of CO_2 compressors and ASU, compared with the EvGT cycle.

Table 4.3 Comparison on electricity generation and internal electricity consumption between combined cycle and EvGT cycle (in % of fuel LHV)

	Without CCS		MEA Absorption		O_2/CO_2 recycle	
	CC	EvGT	CC	EvGT	CC	EvGT
Gross Electricity Generation	95.2	88.5	90.9	71.57	88.5	72
Air/Fuel Compressors	37.6	35.3	37.6	28.2	31.1	23.3
CO_2 Compressors	-	-	2.3	2.18	3.0	2.3
Pumps	0.3	0.04	0.6	0.03	0.3	0.03
ASU	-	-	-	-	6.4	7.4
Auxiliaries	0.6		2.5	-	0.6	-
Net electricity Efficiency	56.7	51.6	47.9	39.73	47.0	37.5

4.3 Economic Evaluation on Various Systems

Based upon a gas turbine, LM1600PD, which capacity is 13.78MW and produced by GE Energy Aeroderivative [86], a preliminary economic calculation was made regarding those three systems. This gas turbine was considered because it has similar performance (turbine exit temperature (TET) and pressure ration) to the turbine simulated in Section 4.2.

4.3.1 Assumptions

The assumptions made in the cost calculation are listed in Table 4.4. The fuel price is the average of Mott MacDonald's long-run forecast prices up to 2025 for the Netherlands coastal location [87]. The Operation & Maintenance cost per year is referred to the total capital cost. And the other fee includes the operating labours cost, local taxation and insurance, and the auxiliary devices which are not involved in the main equipment list. This is also referred to as the capital cost.

Table 4.4 Assumptions made in the cost calculation

Parameter	Unit	Value
Natural Gas Price	USD/kg	0.4 [87]
Interest Rate	per year	8%
Operating Life	year	20
Operating Hours	hr/yr	7500
Operation & Maintenance	%	4 [88]
Other Fee	%	10
MEA Price	USD/kg	1.5 [89]
TEG Price	USD/kg	1 [90]
Make-up Water	USD/ton	1 [91]
Cooling Water (288.15K)	USD/ton	0.2 [91]

4.3.2 Capital Costs and Cost of Electricity

Table 4.5 summarizes the annual costs of different systems. The equipment purchase cost is calculated by CAPCOST [91]. Detailed results are listed in Appendix B. Due to the efficiency penalty and additional equipment for CO_2 capture, System II and III have higher electricity prices than System I. Meanwhile, compared to System III, although System II has a higher annual cost, it has a lower electricity price because of its higher efficiency. However, considering its lower CO_2 capture ratio, System II has a higher specific cost to capture CO_2.

Table 4.5 Annual costs of different systems

	System I	System II	System III
Amortized Capital Cost (kUSD)	2698	2970	2890
O&M (kUSD)	421	463	451
Fuel (kUSD)	3348	4158	4136
MEA (kUSD)	0	86	0
TEG (kUSD)	0	12	12
Make-up Water (kUSD)	53	53	64
Cooling Water (kUSD)	508	508	578
Total (kUSD)	7028	8250	8131
Electricity (USD/kWh)	0.13	0.20	0.21
CO_2 Capture (USD/tonCO_2)	0	47.62	38.89

Figure 4.7 shows the breakdown of CO_2 capture costs of System II and III. It is apparent that the O&M is similar in the two systems. Meanwhile, the main components in the overall capture costs of both methods come from the fuel, due to their large electrical efficiency penalties caused by CO_2 capture. This implies that, to EvGT cycles, improving the cycle efficiency is an important way to reduce the capture cost.

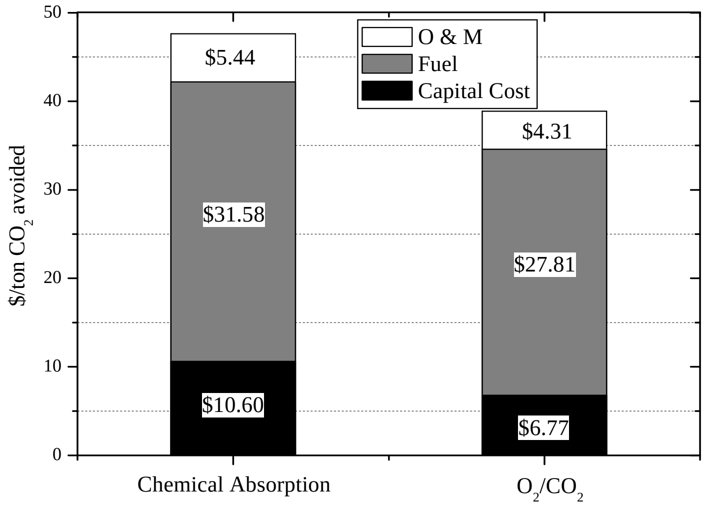

Figure 4.7 Comparison of capture costs of chemical absorption and O_2/CO_2

There have been some studies examining the capture cost from both coal power plants [84-86] and gas turbine cycles [92-94]. Figure 4.8 compares the different results in terms of \$/ton CO_2 captured from different systems. Results from Singh [95], Alston [96], Simbeck [97] and Bill [98] are included. First of all, the systems with chemical absorption in all studies are more expensive than the oxy-fuel combustion-based capture systems. Secondly the results on CO_2 capture costs of this study are similar to those from coal power plants, while larger than those of Bill, which are obtained from combined cycle. The big differences of CO_2 capture costs between CC and EvGT mainly come from the big differences of electrical efficiency, for example, 8.2 and 9.5 percentage point (Table 4.4) for chemical absorption capture and oxy-fuel combustion capture respectively.

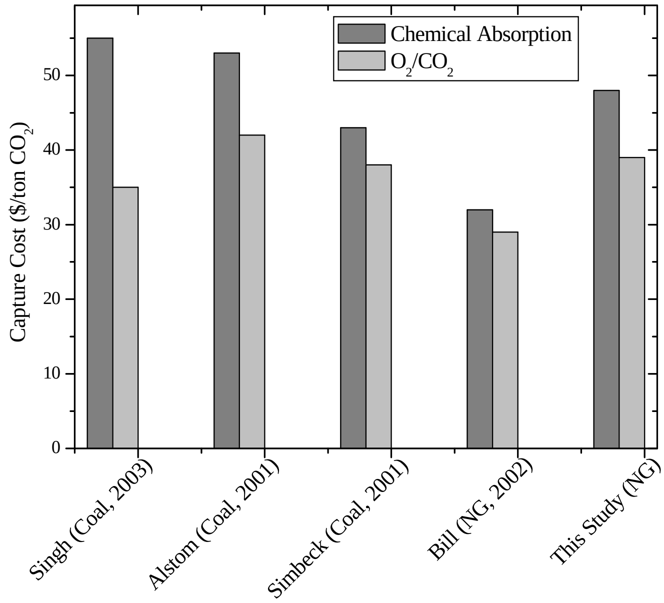

Figure 4.8 Comparison of CO_2 capture costs

4.4 Investigation of EvGT Integrated with MEA Based Chemical Absorption Capture Regarding Electrical Efficiency

In order to improve the electrical efficiency of EvGT cycle integrated with MEA based CO_2 capture technology, three important parameters, including Water/Air ratio (W/A), stripper pressure (STP), and flue gas condensing temperature (FCT), were investigated in a row in this study. The initial values of STP and FCT are 0.1MPa and 313.15K respectively. After one parameter is optimized, the optimal value would be used in the following work. All simulations were conducted with Aspen Plus.

4.4.1 Water/Air Ratio

Water/Air ratio (W/A), which is defined as:

$$W/A = \frac{\text{Mass flow of evaporated water}}{\text{Mass flow of Air}} \tag{4.4}$$

It has been verified that there is always an optimum point. This point occurs when both the air temperature after the recuperation reaches the highest value, and at the same time, the stack temperature is at the lower limit [99]. Figure 4.9 shows the results of the optimization of water/air ratio regarding the EvGT without and with CO_2 capture. Both electrical efficiencies first rise; and then, drop along with the increase of W/A. The highest efficiencies are 52.1% and 41.3%, which were reached at the W/A with values of 0.14 and 0.115 respectively. Different from the impact of W/A on the total efficiency, the efficiency penalty rises along with the increase of W/A.

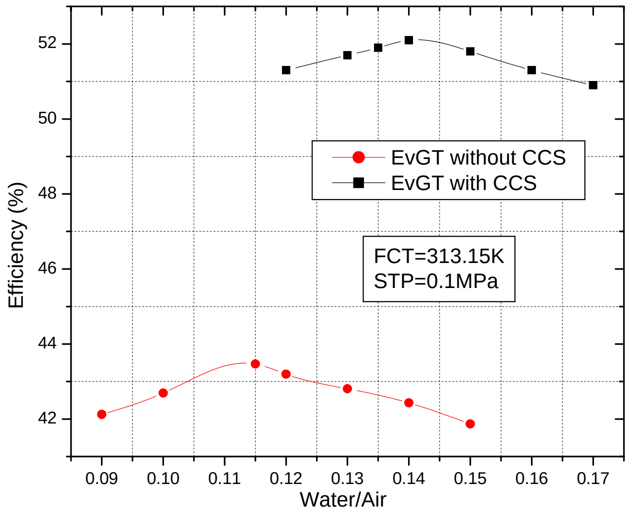

Figure 4.9 Electrical efficiency of EvGT without/with CO_2 capture at different Water/Air ratio

4.4.2 Stripper Pressure

It has been concluded that increasing the stripper operating pressure would increase the stripper operating temperature; while decrease the reboiler duty required for MEA regeneration [83]. This implies that, at a higher operating pressure, the reboiler of stripper may require less heat but in a higher temperature. Therefore, from the viewpoint of exergy, the heat recovered back to the combustor through economizer and humidification tower and the heat required by stripper shall be carefully arranged with the consideration of temperature matching in the heat exchanging processes. This may reduce the irreversibility caused by heat transfer, and result in different overall efficiencies of cycle.

Figure 4.10 shows the specific energy requirements to capture 1ton CO_2 and the reboiler temperatures at different STP. Along with the rise of stripper pressure, the energy requirement decreases; while the reboiler temperature increases. In addition, compared with its reboiler temperature, reboiler duty is more sensitive to the variation of STP if STP is lower than 0.1MPa.

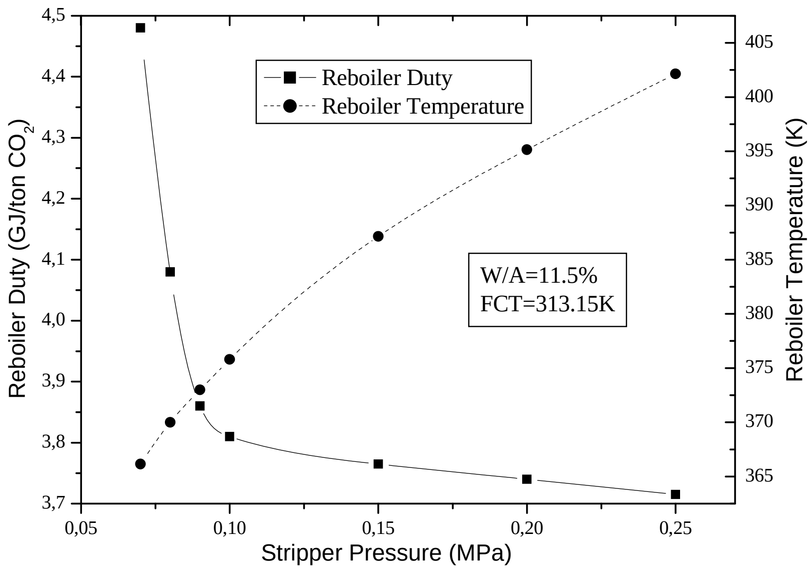

Figure 4.10 Specific energy requirement and reboiler temperature at different stripper pressures

Considering the temperature match in the heat exchangers, two configurations (Figure 4.11) for humidification tower and CO_2 capture were applied regarding the different heat quality and quantity requirements. At low STP, for example 0.07MPa, the reboiler temperature is approximately 366.15K, which is close to the water temperature entering economizer (353.15K). Thus, Configuration 1 would be applied. On the contrary, at high STP, for example 0.25MPa, the reboiler temperature is approximately 401.15K, which is close to the water temperature leaving economizer (420.15K). Thus, Configuration 2 would be applied.

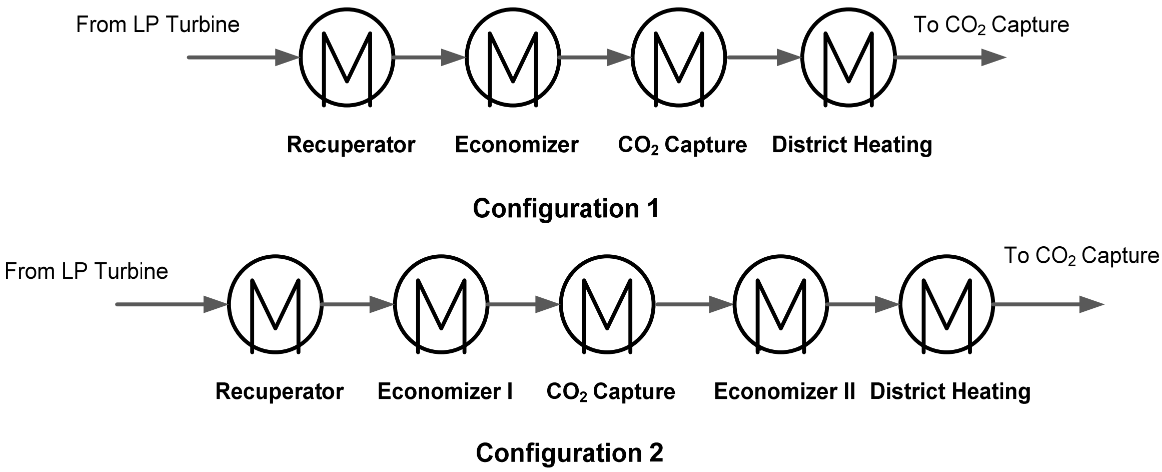

Figure 4.11 Configuration of heat exchangers

According to the above strategy, the results of electrical efficiency at different STP are shown in Figure 4.12. Although the low temperature heat can be used when STP is low, and exergy loss caused by high temperature difference of heat transfer may be reduced by applying different configurations of heat exchangers, electrical efficiency grows with the raise of stripper pressure. The reason is due to the fast increase of reboiler duty at low STP. Therefore, high STP is helpful to improve the total efficiency. Moreover, it is similar to the impact of STP on reboiler duty that efficiency is less sensitive to the variation of STP when it is over 0.2MPa. Therefore 0.2MPa was applied in the following calculations, in order to avoid the quick increment of investment costs caused by the raise of stripper pressure.

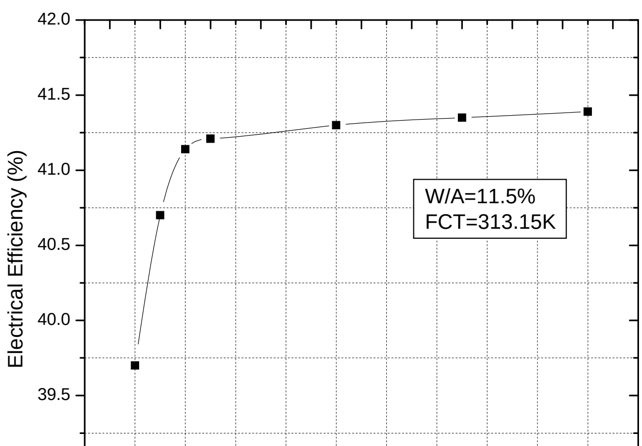

Figure 4.12 Electrical efficiency at different stripper pressures

4.4.3 Flue Gas Condensing Temperature

In Section 4.2.2, the heat required for MEA regeneration in System II is 3.84GJ/ton CO_2, which is higher than the value 3.45GJ/ton CO_2 given in [83]. It has been known that the heat demand decreases with increasing MEA concentration [83]. Since System II is a humidified gas turbine cycle, more water is contained in the CO_2 stream entering CO_2 absorber compared to the conventional gas turbine cycles. The excessive water would dilute MEA solvent, and result in a higher reboiler duty. Therefore, decreasing the water content in the CO_2 stream can help reduce the thermal energy requirement of reboiler. In order to remove excessive water, flue gas should be condensed before entering absorber. The variation of condenser temperature would firstly change the reboiler duty of striper, and further affect the distribution of heat recovery in humidification and economizer. As a result, the total efficiency would be changed.

Figure 4.13 shows the specific reboiler duty of stripper at different condenser temperatures. When the condenser temperature drops from 333.15K to 323.15K, more water is condensed, so reboiler duty is reduced. However, when condenser temperature drops further, reboiler duty may increase. The reason for this might be that the low condenser temperature would cause a low input temperature of reboiler. Although less water is contained, the larger temperature difference between inlet temperature and operation temperature will increase the reboiler duty.

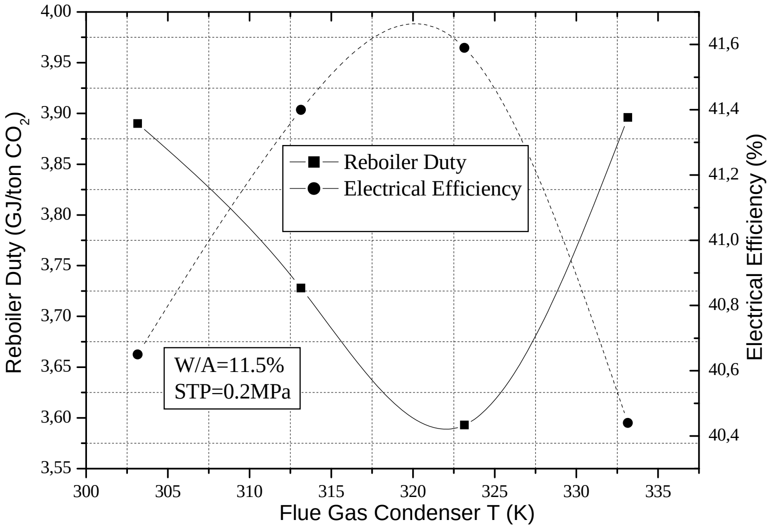

Figure 4.13 Specific reboiler duty and electrical efficiency at different condenser temperatures

Figure 4.13 also shows the electrical efficiency at different condenser temperature. FCT has a reverse impact on efficiency compared its impact on reboiler duty. In this study, the highest electrical efficiency appears with a value of 41.6% when FCT is 323.15K.

4.5 Discussions

4.5.1 Economic Benefit

As indicated in Figure 4.5, much heat can be recovered for district heating from EvGT cycles. However, the economic benefit from heat recovery was not included in the economic evaluation performed in Section 4.3, because it was not included in other studies either. If it could be counted, the cost to capture 1 ton CO_2 would be further reduced.

4.5.2 Optimization Regarding EvGT + CO_2 Capture

According to the optimization result of EvGT + chemical absorption, increasing the operating pressure of stripper and adding a flue gas condenser would help to increase the total electrical efficiency. However, the increased pressure and additional condenser would raise the investment costs at the same time. Therefore, the economic comparison should be conducted in any future work in order to understand more comprehensively the integration of EvGT with CO_2 capture.

In addition, to the system of EvGT + O_2/CO_2, more impurities are expected in the CO_2 streams to be transported. However, there are restrictions for different transport conditions based upon Table 3.5. To control the impurity fraction under the acceptable value, an additional purification system might be required. Under such a situation, EvGT + O_2/CO_2 may have a CO_2 capture cost close to EvGT + chemical absorption.

4.5.3 Future Work

The system performance of EvGT + chemical absorption has been investigated. The same work should be conducted regarding EvGT + O_2/CO_2. Based upon those investigation results, further economic evaluation should be performed to obtain more accurate comparison of both systems.

5 Conclusions

In the first part of this thesis, the thermodynamic properties of CO_2 mixtures have been studied, including the evaluations of various calculation methods and the investigations of the impacts of impurities on the properties of mixtures and different processes involved in CCS.

The results show that:

- There are some gaps of the experimental data on the thermodynamic properties of CO_2 mixtures. The available data cannot cover the operation conditions of different the CCS processes, which may result in a limited reliability of the evaluation results of theoretical modelling.
- EOS method is better than activity coefficient method in calculations of thermodynamic properties of CO_2 mixtures; and the reliabilities of EOS vary for the components, the properties, such as VLE and volume, and the calculating conditions.
- For the thermodynamic property calculations of binary CO_2 mixtures, cubic EOS is more applicable from the viewpoint of engineering application. To VLE properties, comparatively PR is recommended for the calculations of CO_2/CH_4 and CO_2/H_2S; PT is recommended for the calculations of CO_2/O_2, CO_2/N_2 and CO_2/Ar; while 3P1T is recommended for the calculations of CO_2/SO_2. To volume properties, PT is recommended for the calculations of CO_2/CH_4, V_l of CO_2/H_2S, CO_2/Ar and CO_2/SO_2, and V_g of CO_2/N_2; PR is recommended for the calculations of V_l of CO_2/N_2 and V_g of CO_2/Ar; MPR and ISRK are recommended for the calculations of V_l of CO_2/H_2S and V_g of CO_2/SO_2 respectively.
- Calibrated k_{ij} can improve the accuracy of VLE calculation; however it doesn't mean the k_{ij} calibrated from VLE data will definitely result in a higher accuracy on the volume calculation as well. Therefore, it is recommended to separate the calculation of thermodynamic properties into two parts: VLE calculation and volume calculation. In different cases, various EOS with various parameters should be chosen.
- Impurities have great impacts on the design, operation, and optimization of the CCS system through their impacts on the thermodynamic properties of CO_2 streams: (1) the presence of SO_2 makes the heat capacities of CO_2 mixtures raise while the presence of O_2, Ar and N_2 makes them decrease. As a result, the enthalpy and entropy of CO_2 streams are increased with the increment of SO_2, while decreased with the increment of O_2, Ar and N_2; (2) the presence of non-condensable gases makes condensation more difficult; thus, resulting in increased pressure requirements for the condensation of the CO_2 mixtures. Comparatively the operation conditions are more sensitive to the concentration variations of N_2 than those of O_2 and Ar; (3) theoretically the isothermal compression work, the discharging temperature of isentropic compression and the isentropic compression work are increased with the increments of mole fractions of O_2, Ar and N_2; yet they are decreased with the increment of SO_2 linearly at the same discharging pressure. Comparatively the isothermal compression work is more sensitive to the concentration variations of SO_2; while the isentropic compression work is more sensitive to the concentration variations of Ar; (4) energy consumption of external refrigeration is increased with the increments of mole fractions of SO_2, while decreased with the increment of Ar, O_2 and N_2; and (5) the existence of impurities would reduce the transported mass of CO_2 and result in lower transport efficiency and storage capacity. The occupied volumes by the given concentrations of impurities in corresponding CO_2 mixtures are in following order: $V_{N2} > V_{O2} > V_{Ar} > V_{SO2}$.

In the second part of this thesis, the performances of EvGT cycles integrated with various CO_2 capture technologies have been analyzed, including the technical and economical evaluations.

The results show that:

- The EvGT cycle + chemical absorption capture has a higher electrical efficiency, while a smaller amount of heat recovered for the district heating than the EvGT cycle + O_2/CO_2 recycle combustion capture;
- Compared with the EvGT cycle without CO_2 capture, the EvGT + chemical absorption capture has a smaller penalty on electrical efficiency than the EvGT + O_2/CO_2 recycle combustion capture;
- The EvGT cycle + O_2/CO_2 recycle combustion has a higher CO_2 capture ratio and lower CO_2 emissions per kWh produced electricity than the EvGT cycle + chemical absorption capture;
- Comparatively; the combined cycle has a higher gross electricity generation and electrical efficiency than the EvGT cycle regardless if it is combined with CO_2 capture; while the difference is smaller if CO_2 is captured through chemical absorption;
- Compared to the EvGT + O_2/CO_2, although the EvGT + chemical absorption has a higher annual cost, it has a lower electricity price because of its higher efficiency. However considering its lower CO_2 capture ratio, the EvGT + chemical absorption has a higher cost to capture 1 ton CO_2.
- There exists an optimum point of W/A for both the EvGT and the EvGT combined with CCS. As TIT=1523.15K and pressure ratio=20, the optimal W/A is 14.0% and 11.5% for the EvGT and the EvGT + chemical absorption respectively
- To the EvGT + chemical absorption, increasing the operating pressure of stripper would help increase the total electrical efficiency; however, the efficiency improvement becomes smaller if stripper pressure is high. Meanwhile adding a flue gas condenser condensing out the excessive water is another method to increase the total electrical efficiency. There is also an optimum point of condensing temperature, considering the concentration of MEA and inlet temperature of stripper.

Appendix:

A: Flow chart of calibrating k_{ij}

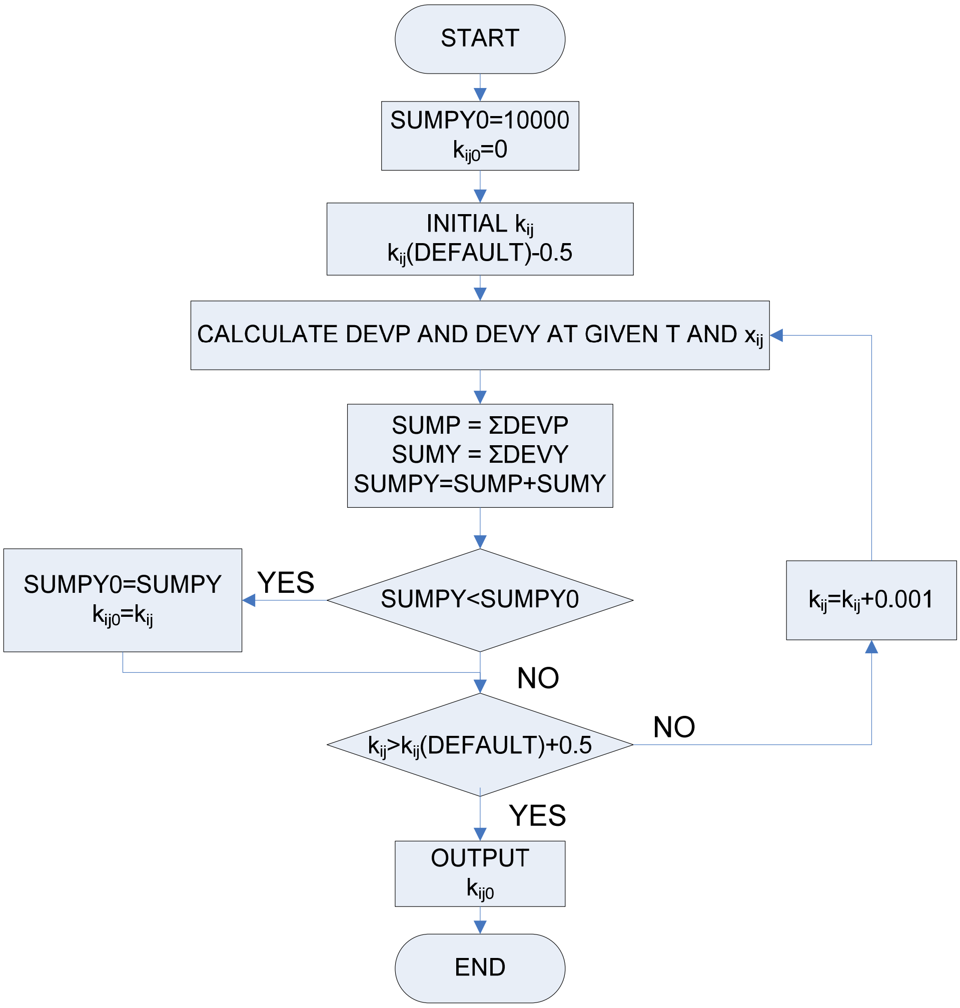

Figure A- 1 Flow chart of regressing k_{ij}

B: Summary of capital costs of EvGT and EvGT + CCS.

Table A- 1 Capital costs of EvGT without CCS

Equipment	NO	Capacity	Type	Material	Key parameter	Capital cost kUSD
Air Compressor (1st stage)	C-101	2.43 MW	Axial	SS		522
Air Compressor (2nd stage)	C-102	2.98 MW	Axial	SS		597
Fuel Compressor	C-103	283 kW	Axial	SS		150
Gas Turbine [86]	J-101	13.78 MW	Axial	SS	LM1600PD	7000
Water pump	P-101	5.97 kW	Centrifugal	SS		3.34
Combustor	H-101	19.2 MW		CS		1780
Intercooler of air compression	E-101	2.11 MW	T-S	SS	h=0.7 kW/m^2C	39.6
Aftercooler	E-102	2.07 MW	T-S	SS	h=0.7 kW/m^2C	35.1
Recuperator	E-103	7.40 MW	FP	SS	h=0.4 kW/m^2C	173
Economizer	E-104	2.31 MW	T-S	SS	h=0.7 kW/m^2C	22.6
Heat recovery for district heating	E-105	2.55 MW	T-S	SS	h=0.7 kW/m^2C	30.9
Flue Gas Condenser	E-106	4.62 MW	T-S	SS	h=0.7 kW/m^2C	35.4
Humidification Tower [85]				SS		136.2
Total						10525.14

Table A- 2 Capital costs of EvGT with chemical absorption capture

Equipment	NO	Capacity	Type	Material	Key parameter	Capital cost kUSD
Air Compressor (1st stage)	C-101	2.43 MW	Axial	SS		522
Air Compressor (2nd stage)	C-102	2.98 MW	Axial	SS		597
Fuel Compressor	C-103	283 kW	Axial	SS		150
Compressor of dehydration	C-104	364 kW	Rotary	SS		689
CO_2 compressor	C-105	169 kW	Rotary	SS		133
Gas Turbine	J-101	13.78 MW	Axial	SS	LM1600PD	7000
Water pump	P-101	5.97 kW	Centrifugal	SS		3.34
Combustor	H-101	19.2 MW		CS		1780
Absorber	T-101			SS	15 sieve layer, H=15 m, D=2.51 m	98.5
Stripper	T-102			SS	10 sieve layer, H=10 m, D=1.18	22.3
Dehydration column	T-103			SS	10 sieve layer, H=5 m, D=2 m	36
TEG regeneration column	T-104			SS	10 sieve layer, H=5 m, D=24 m	48.7
Intercooler of air compression	E-101	2.11 MW	T-S	SS	h=0.7 kW/m²C	39.6
Aftercooler	E-102	2.07 MW	T-S	SS	h=0.7 kW/m²C	35.1
Recuporator	E-103	3.79 MW	FP	SS	h=0.4 kW/m²C	63.5
Economizer	E-104	2.39 MW	T-S	SS	h=0.7 kW/m²C	21.8
Heat recovery for district heating	E-105	3.10 MW	T-S	SS	h=0.7 kW/m²C	33.8
Flue Gas Condenser	E-106	3.60 MW	T-S	SS	h=0.7 kW/m²C	35
Stripper economizer	E-107	2.48 MW	T-S	SS	h=1.5 kW/m²C	22.9
Stripper reboiler	E-108	3.64 MW	T-S	SS	h=0.7 kW/m²C	38.5
Stripper condenser	E-109	1.00 MW	T-S	SS	h=0.7 kW/m²C	24.8
Dehydration condenser	E-110	0.647 MW	Air cooler	SS	h=0.3 kW/m²C	20.8
CO_2 condenser	E-111	0.425 MW	T-S	SS	h=0.7 kW/m²C	15.3
Dehydration reboiler	E-112	1.33 MW	T-S	SS	h=0.7 kW/m²C	18.9
Humidification Tower				SS		136.2
Total						11586.04

Table A- 3 Capital costs of EvGT with O_2/CO_2

Equipment	NO	Capacity	Type	Material	Key parameter	Capital cost kUSD
Air Compressor (1st stage)	C-101	2.15	Axial	SS		481
Air Compressor (2nd stage)	C-102	2.31	Axial	SS		505
Fuel Compressor	C-103	0.282	Axial	SS		150
Compressor of dehydration	C-104	324 kW	Rotary	SS		523
CO_2 compressor	C-105	101 kW	Rotary	SS		46.4
Gas Turbine	J-101	13.78 MW	Axial	SS	LM1600PD	7000
Water pump	P-101	6.51 kW	Centrifugal	SS		3.43
Combustor	H-101	19.2MW		CS		1780
Dehydration column	T-103			SS	10 sieve layer, H=5 m, D=2 m	36
TEG regeneration column	T-104			SS	10 sieve layer, H=5 m, D=24 m	48.7
Intercooler of air compression	E-101		T-S	SS	h=0.7 kW/m^{2}C	37.1
Aftercooler	E-102		T-S	SS	h=0.7 kW/m^{2}C	17.5
Recuporator	E-103		FP	SS	h=0.4 kW/m^{2}C	105
Economizer	E-104		T-S	SS	h=0.7 kW/m^{2}C	22.1
Heat recovery for district heating	E-105		T-S	SS	h=0.7 kW/m^{2}C	43.5
Flue Gas Condenser	E-106		T-S	SS	h=0.7 kW/m^{2}C	33.3
Dehydration condenser	E-110		Air cooler	SS	h=0.3 kW/m^{2}C	20.8
CO_2 condenser 1						15.3
CO_2 condenser 2	E-111		T-S	SS	h=0.7 kW/m^{2}C	15.3
Dehydration reboiler	E-112		T-S	SS	h=0.7 kW/m^{2}C	18.9
Humidification Tower				SS		136.2
ASU [100]						235.74
Total						11274.27

References

[1] Intergovernmental Panel on Climate Change (IPCC), *Climate change 2007: The physical science basis, summary for policymakers*, Feb 2007.

[2] United Nations Framework Convention on Climate Change (UNFCCC), http://unfccc.int/essential_background/feeling_the_heat/items/2917.php

[3] Intergovernmental Panel on Climate Change (IPCC), *Climate Change 2001: Synthesis report*, Cambridge University Press, Cambridge, UK, 2001.

[4] Stangeland A. Why CO_2 capture and storage (CCS) is an important strategy to reduce global CO_2 emissions, The Bellona Foundation, June 1, 2007, also see: http://www.bellona.org/filearchive/fil_Bellona_Paper_-_Why_CCS_-_1June07.pdf

[5] Intergovernmental Panel on Climate Change (IPCC), *IPCC Special Report on Carbon Dioxide Capture and Storage*, Cambridge University Press, 2005

[6] Abbott M.M. Cubic equations of state: an iterative review. *Am. Chem. Soc. Adv. Chem. Ser.* 182:47-70, 1979.

[7] Danesh A., Xu D-H., Todd A.C. Comparative study of cubic equations of state for predicting phase behavior and volumetric properties of injection gas-reservoir oil systems. *Fluid Phase Equilibria* 63:259-278, 1991.

[8] Yang J., Griffiths P.R., Goodwin A.R.H., Comparison of methods for calculating thermodynamic properties of binary mixtures in the sub and super critical state: Lee-Kesler and cubic equations of state for binary mixtures containing either CO_2 and H_2S. *J. Chem. Thermodynamics* 35:1521-1539, 2003.

[9] Peng D.Y., Robinson D.B. A new two-constant equation of state. *Ind. Eng. Chem. Fundam.* 15:59–64, 1976.

[10] Soave G. Equilibrium constants for modified Redlich-Kwong equation of state. *Chemical Engineering Science* 27:1196-1203, 1972.

[11] Carrol J.J., Lui D.W. Equations for evaluating acid gas injection. *Oil & Gas Journal* 6:64-72, 1997.

[12] Carroll J.J., Maddocks J.R. Design considerations for acid gas injection. In: *Proceedings of Laurance Reid Gas Conditioning Conference*. Norman Oklahoma, USA. Feb 1999.

[13] Bernstone C., Yan J., von Dalwigk I., Liljemark S. Identifying potential temperature, pressure and composition windows of CO_2 streams, and major properties of CO_2 mixture used for CCS engineering and system design. *Technical report* (MEMO U 06-91) Vattenfall Research and Development AB, Nov 2006.

[14] Yan J., Liljemark S. A report within the CO_2 free power plant project. *Vattenfall report,* 2004.

[15] Holste J.C., Hall K.R., Eubank P.T., Esper G., Watson M.Q., Warowny W., Bailey D.M., Young J.G. Bellomy M.T. Experimental (p, Vm, T) for pure CO_2 between 220 and 450K. *J. Chem. Thermodynamics* 19:1233-1250, 1987.

[16] Ernst G., Hochberg E.U. Flow-calorimeter for the accurate determination of the isobaric heat capacity at high pressures, results for carbon dioxide. *J. Chem. Thermodynamics* 21:53-65, 1989.

[17] Duschek W., Kleinrahm R., Wanger W. Measurement and correlation of the (pressure, density, temperature) relation of carbon dioxide I. The homogeneous gas and liquid regions in the temperature range from 217 K to 340 K at pressures up to 9 MPa. *J. Chem. Thermodynamics* 22:827-840, 1990.

[18] Gilgen R., Kleinrahm R., Wagner W. Supplementary measurements of the (pressure, density temperature) relation of carbon dioxide in the homogeneous region at temperatures from 220K to 360K and pressures up to 13MPa. *J. Chem. Thermodynamics* 24:1243-1250, 1992.

[19] Brachthäuser K., Kleinrahm R., Lösch H.W., Wagner W. Entwicklung eines neuen Dichtemeßverfahrens und Aufbau einer *Hochtemperatur-Hochdruck-Dichtemeßanlage. VDI-Verlag.* Düsseldorf, 1993.

[20] Möller D., Gammon B.E., Marsh K.N., Hall K.R., Holste J.C. Enthalpy-increment measurements from flow calorimetry of CO_2 and of $\{xCO_2+(1-x)C_2H_6\}$ from pressures of 15 MPa to 18 MPa between the temperatures 230 K and 350 K. *J. Chem. Thermodynamics* 25:1273-1279, 1993.

[21] Fenghour A., Wakeham W.A., Waston J.T.R. Amount-of-substance density of CO_2 at temperatures from 329 K to 698 K and pressures up to 34MPa. *J. Chem. Thermodynamics* 27:219-223, 1995.

[22] Klimeck J., Kleinrahm R., Wagner. W. Measurements of the (p, ϱ, T) relation of methane and carbon dioxide in the temperature range 240K to 520K at pressures up to 30MPa using a new accurate single-sinker densimeter. *J. Chem. Thermodynamics* 33:251-267, 2001.

[23] Caubet F. Liquéfaction des mélanges gazeux, Université de Bordeaux, 1901.

[24] Reamer H.H., Olds R.H., Sage B.H., Lacey W.N. Phase equilibria in hydrocarbon systems: methane-carbon dioxide system in the gaseous region. *Industrial and Engineering Chemistry* 35(1):88-90, 1944.

[25] von Steckel F. Dampf-Flussigkeits-Gleichgewichte einiger binarer, schwefelwasserstoffhaltiger systeme unter Druck, Svensk *Kemisk Tidskrift* 9:209-216, 1945.

[26] Bierlein J.A. Kay W.B. Phase-equilibrium properties of system carbon dioxide-hydrogen sulfide, *Industrial and Engineering Chemistry* 45(3):618-624, 1953.

[27] Donnelly H.G., Katz D.L., Phase equilibria in the carbon dioxide-methane system. *Industrial and Engineering Chemistry* 46(3):511-517, 1954.

[28] Muirbrook N.K., Prausnitz J.M. Multicomponent Vapor-Liquid Equilibria at High Pressures: Part I Experimental study of the nitrogen-oxygen-carbon dioxide system at 0^oC. *A.I.Ch.E. Journal* 11(6):1097-1102, 1965.

[29] Chuen P.L., Muirbrook N.K., Prausnitz J.M. Part II. Thermodynamic Analysis, *A. I. Ch. E. Journal*, 11(6):1092-1097, 1965.

[30] Kestin J., Kobayashi Y., Wood R.T. The Viscosity of Four Binary Gaseous Mixtures at 20 and 30 C, *Physica Amsterdam* 32:1065-1089, 1966.

[31] Greenwood H.J. The compressibility of gaseous mixtures of carbon dioxide and water between 0 and 500 bars pressure and 450 ° and 800 ° centigrade. *Am. J. Sci.* 267A:191-208, 1969.

[32] Fredenslund A., Sather G.A. Gas-liquid equilibrium of the oxygen-carbon dioxide system. *Journal of Chemical and Engineering Data* 15(1):17-22, 1970.

[33] Arai Y., Kaminishi G., Saito S. The experimental determination of the P-V-T-X relations for the carbon dioxide-nitrogen and the carbon dioxide-methane system. *Journal of Chemical Engineering of Japan* 4(2):113-122, 1971.

[34] Sarashina E., Arai Y., Saito S. The P-V-T-X Relation for the Carbon Dioxide – System. *J. Chem. Eng. Jpn.* 4:379-381, 1971.

[35] Davalos J., Anderson W.R., Phelps R.E., Kldnay A.J. Liquid-vapor equilibria at 250.00K for systems containing Methane, Ethane, and Carbon Dioxide. *Journal of Chemical and Engineering Data* 21(1):81-84, 1976.

[36] Altunin V.V., Koposhilov O.D. An experimental study of thermal properties of gaseous mixtures of carbon dioxide with argon, *Teploenergetika* 24(8):80-83, 1977.

[37] Mraw S.C., Hwang S., Kobayashi R. Vapor-liquid equilibrium of the CH_4-CO_2 system at low temperature. *Journal of Chemical and Engineering Data* 23(2):135-139, 1978.

[38] Somait F.A., Kidnay A.J. Liquid-vapor equilibria at 270.00K for system containing nitrogen, methane, and carbon dioxide. *Journal of Chemical and Engineering Data* 23(4):301-305, 1978.

[39] Zawisza A., Malesinska B. Solubility of carbon dioxide in liquid water and of water in gaseous carbon dioxide in the range 0.2-5 MPa and at temperatures up to 473K. *J. Chem. Eng. Data* 26(4):388-391, 1981.

[40] Dorau W.I., Al-Wakeel M., Knapp H. VLE data for CO_2-CF_2Cl_2, N_2-CO_2, N_2-CF_2Cl_2 and N^2-CO_2-CF_2Cl, *Cryogenics* 29-35, 1983.

[41] Patel M.R., Eubank P.T. Experimental densities and derived thermodynamic properties for carbon dioxide-water mixtures. *J. Chem. Eng. Data* 33:185-193, 1988.

[42] Esper G.J., Bailey D.M., Holste J.C., Hall K.R. Volumetric behavior of near-equimolar mixtures for CO_2+CH_4 and CO_2+N_2. *Fluid Phase Equilibria* 49:35-47, 1989.

[43] Sterner S.M., Bodnar R.T. Synthetic fluid inclusions. X. Experimental determination of P-V-T-X properties in the CO_2-H_2O system to 6 KB and 700 °C. *Am. J. Sci.* 291:1-54, 1991.

[44] Fenghour A., Wakeham W.A., Watson J.T.R. Isochoric density measurements of dense gaseous mixtures of carbon dioxide and water. *High Temperature-High Pressure* 26:241-250, 1994.

[45] Seitz J.C., Blencoe J.G. The CO_2-H_2O system. I. Experimental determination of volumetric properties at 400 °C, 10-100 MPa. *Geochimica et Cosmochimica Acta.* 63(10):1559-1569, 1999.

[46] Aspen ONE 2006, Aspen technology Inc., Cambridge, MA, USA.

[47] Twu C.H., Coon J.E., Kusch M.G., Harvey A.H. Selection of equations of state models for process simulation. *Simulation Science*, Inc., 601 South Valencia Avenue, Brea, CA 92621, USA, 1994.

[48] Standler S.I., Orbey H., Lee B.-I. Chapter 2: equation of state, *In Models for Thermodynamic and Phase Equilibria Calculations.* Edited by Sandler, S.I., Marcel Dekker, Inc. New York, 1994.

[49] Span R., Wagner W. A new equation of state for carbon dioxide covering the fluid region from the triple-point temperature to 1100K at pressures up to 800MPa. *J. Phys. Chem. Ref. Data* 25(6):1509-1596, 1996.

[50] van der Waals J.D. Over de continuiteit van den gas – en vloestoftoestand. Dissertation, Leiden University, Leiden, Netherland, 1873.

[51] Redlich O., Kwong J.N.S. On the thermodynamics of solutions. *Chem. Rev.* 44:233-244, 1949.

[52] Benedict M., Webb G.B., Rubin L.C. An empirical equation for thermodynamic properties of light hydrocarbons and their mixtures. *J. Chem. Phys.* 8:334, 1940.

[53] IPSEpro, SimTech Simulation Technology, Austria.

[54] Bottinga Y., Richet P. High pressure and temperature equation of state and calculation of the thermodynamic properties of gaseous carbon dioxide. *American Journal of Science* 281(5):615–660, 1981.

[55] Patel N.C., Teja A.S. A new cubic equation of state for fluids and fluid mixtures. *Chemical Engineering Science* 37(3):463-473, 1982.

[56] Soave G. Equilibrium constants for modified Redlich-Kwong equation of state. *Chemical Engineering Science* 27:1196-1203, 1972.

[57] Yu J., Lu B.C., Iwai Y. Simultaneous calculations of VLE and saturated liquid and vapor volumes by means of a 3P1T cubic EOS. *Fluid Phase Equilibria* 37:207-222, 1987.

[58] Prausnitz J.M., Lichtenthaler R.N., de Azevedo E.G. *Molecular thermodynamics of fluid-phase equilibria*. 2nd edition, Prentice-Hall, 1986

[59] Moysan J., Huron M., Paradowski H., Vidal J. Prediction of the solubility of hydrogen in hydrocarbon solvents through cubic equation of state for fluids and fluids mixtures *Chem. Eng. Sci.* 77(3), 463-473, 1983

[60] Voros N.G., Tassios D.P. Vapor-liquid equilibria in non-polar/weakly polar systems with different types of mixing rules. *Fluid Phase Equilibria* 91:1-29, 1985.

[61] Bjorlykke O.P., Firoozabadi A. Measurement and computation of retrograde condensation and near critical phase behavior, In: *Proceedings of SPE Annual Technocal Conference and Exhibition, EOR volume*, SPE 20524, 541-550, 1990

[62] Hu J., Duan Z., Zhu C., Chou I. PVTx properties of the CO_2-H_2O and CO_2-H_2O-NaCl systems below 647K: assessment of experimental data and thermodynamic models. *Chem. Geo.* 238:249-267, 2007.

[63] Ji Y., Ji X., Feng X., Liu C., Lu L., Lu X. Progress in the study on the phase equilibria for the CO_2-H_2O and CO_2-H_2O-NaCl systems. *Chin. J. Chem. Eng.* 15(3):439-448, 2007.

[64] Peneloux A., Rauzy E. A consistent correction for Redlich-Kwong-Soave volumes. *Fluid Phase Equilibria* 8:7-23, 1982.

[65] Ji W., Lempe D.A. Density improvement of the SRK equation of state. *Fluid Phase Equilibria* 130(1-2):49-63, 1997.

[66] Yan J., Anheden M., Lindgren G., Stroberg L. Conceptual Development of Flue Gas Cleaning for CO_2 Capture from Coal-fired Oxyfuel Combustion Power Plant. In: *Proceedings of 8th International Conference on Greenhouse Gas Control Technologies*, Trondheim, Norway, 2006.

[67] Perry R.H., Green D.W. *Perry's chemical engineering handbook (7th Edition)*. McGraw-Hill, 1997.

[68] McCabe W.L., Smith J.C. *Unit Operations of Chemical Engineering*. McGraw-Hill Kogakusha, Ltd, 1976.

[69] Shao Y., Golomb D., Brown G. Natural gas fired combined cycle power plant with CO_2 capture. *Energy Convers. Mgmt.* 36(12): 1115-1128, 1995.

[70] Bolland O., Mathieu P. Comparison of two CO_2 removal options in combined cycle power plants. *Energy Convers. Mgmt.* 39(16-18): 1653-1663, 1998.

[71] Bolland O., Undrum H. A novel methodology for comparing CO_2 capture options for natural gas-fired combined cycle plants. *Adv Environ Res.* 7:901-911, 2003.

[72] Kvamsdal H.M., Jordal K., Bolland O. A quantitative comparison of gas turbine cycles with CO_2 capture. *Energy* 32: 10-24, 2007.

[73] Jonsson M., Yan J. Humidified gas turbines—a review of proposed and implemented cycles. *Energy* 30(7):1013-1078, 2005.

[74] Arnold D.S., Barrett D.A., Isom R.H. CO_2 can be produced from flue gas. *Oil & Gas Journal* 11:130-136, 1982.

[75] Barchas R., Davis R. The Kerr-McGee/ABB Lummus Crest Technology for the Recovery of CO_2 from Stack Gases. *Energy Convers. Mgmt.* 33(5-8): 333-340, 1992.

[76] Sander M.T., Mariz C.L. The Fluor Daniel ® Econamine™ FG Process: Past Experience and Present Day Focus. *Energy Convers. Mgmt.* 33(5-8): 341-348, 1992.

[77] Chapel D.G., Mariz C.L., Ernest J. Recovery of CO_2 from flues gases: commercial trends, *Annual meeting of the Canadian Society of Chemical Engineering.* Saskatoon, Canada, 1999.

[78] Mimura T., Nojo T., Ijima M., Yoshiyama T., Tanaka H. Recent developments in flue gas CO_2 recovery technology. In: *Proceedings of 6th International Conference on Greenhouse Gas Control Technologies (GHGT-6).* Kyoto, Japan, 2002.

[79] Heitmer F., Jericha H. Graz cycle- an optimized power plant concept for CO_2 retention, First Int Conf on Industrial GT Technologies, *RTD Framework Programme of the European Union*, Brussels, 2003

[80] Mathieu P. Mitigation of CO_2 emissions using low and near zero CO_2 emission power plants. *Int. J. on Energy for a clean Environment* 4: 1-16, 2003.

[81] Panesar R., Gibbins J., Allam R.J., White V.W. A. Oxy-combustion processes for CO_2 capture from power plant. *In Proceedings of 7th International Conference on Greenhouse Gas Control Technologies (GHGT-7),* Vancouver, Canada, 2004.

[82] Pande J.O., Hegerland G., Jorgensen T. Liquefaction and handling large amount of CO_2 for EOR. *In Proceedings of 7th International Conference on Greenhouse Gas Control Technologies (GHGT-7),* Vancouver, Canada, 2004.

[83] Abu-Zahra M., Schneiders L., Niederer J., Feron P., Versteeg G. CO_2 capture from power plants, Part I. A parametric study of the technical performance based on mono-ethanolamine. *Int J. of Greenhouse Gas Control* 1:37-46, 2007.

[84] Nivargi J.P., Gupta D.F., Shaikh S.J., Shah K.T. TEG contactor for gas dehydration, *Chemical Engineering World* 40(9): 77-80, 2005.

[85] Jonsson M., Yan J. Economic assessment of evaporative gas turbine cycles with optimized part flow humidification systems, In: *Proceedings of ASME Turbo Expo.* Atlanta, Georgia, USA, 2003.

[86] Gas Turbine World, *2004-05 GTW Handbook.* Pequot Publishing Inc.

[87] IEA GHG. CO_2 capture as a factor in power station investment decisions. Report 2006-8, *IEA Greenhouse Gas R&D Programme*, Cheltenham, GL52 7RZ, UK, 2006.

[88] Davison J. Performance and costs of power plants with capture and storage of CO_2. *Energy* 32:1163-1176, 2007.

[89] Abu-Zahra M., Niederer J., Feron P., Versteeg G. CO_2 capture from power plants, Part II. A parametric study of the economical performance based on mono-ethanolamine. *Int J. of Greenhouse Gas Control* 1:135-142, 2007.

[90] http://www.icis.com/Articles/2004/08/06/602645/deg-and-teg-prices-surge.html

[91] Turton R., Bailie R.C., Whiting W.B., Shaeiwitz J.A. *Analysis, synthesis, and design of chemical processes (2nd Edition)*. Prentice Hall PTR, 2003.

[92] Siikavirta H. CO_2 capture, transport and storage: cost. Helsinki University of Technology, 2003.

[93] Turkenburg W.C. State of the Art CCS. Copernicus Instituuut voor Duurzame Ontwikkeling en Innovatie, Universiteit Utrecht, 2005.

[94] Li H., Marechal F., Burer M., Favrat D. Multi-objective optimization of an advanced combined cycle power plants including CO2 separation options. *Energy*. 31:3117-3134, 2006.

[95] Singh D., Croiset E., Douglas P.L., Douglas M.A. Techno-economic study of CO_2 capture from an existing coal-fired power plant: MEA scrubbing vs. O_2/CO_2 recycle combustion. *Energy Convers. Mgmt.* 44:3073-3091, 2003.

[96] Nsakala N., Marion J., Guha M., Plasynski S., Johnson H., Gupta J. Engineering feasibility of CO_2 capture on an existing US coal-fired power plant. In: *Proceedings of First Conference on Carbon Sequestration*, Washington DC, United States, 2001.

[97] Simbeck D.R. CO2 migration economics for existing coal-fired power plants. In: *Proceedings of First Conference on Carbon Sequestration*, Washington DC, United States, 2001.

[98] Bill A. Overviews of Techniques and Approaches to CO_2 Capture, ALSTOM Power. http://www.natural-resources.org/minerals/CD/docs/regional/unece/workshop/Bill_Alstom_IEAGHG.ppt

[99] Yan J., Eidensten L., Svedberg G. An investigation of the heat recovery system in externally fired evaporative gas turbines, In: *Proceedings of ASME International Gas Turbine and Aeroengine Congress and Exposition*. Houston, Texas, USA, 1995.

[100] IEA GHG R&D Programme, Leading options for the capture of CO_2 emissions at power stations, Report No. PH3/14, 2000.

Acknowledgements

First and foremost, I would like to thank my supervisor Prof. Jinyue Yan for his continuous support, encouraging and stimulating guidance since the first day.

I must express special gratitude to Dr. Jinying Yan for giving me valuable suggestions.

I would also like to thank Prof. Mats Westmark and Dr. Marie Anheden for useful discussions and help.

There are so many colleagues and friends that I would like to thank, especially those at the Division of Energy Processes for providing a pleasant and creative working environment.

The financial support from the Swedish Energy Agency and Vattenfall is gratefully acknowledged.

Last but not least, my parents deserve my deepest appreciation for always supporting me throughout these years. I would like to thank my dear wife Xiaohui Jia and my lovely daughter Yichen Li for all the happiness they brought to me.

Hailong Li

September 2008